Instituto Tecnológico y de Estudios Superiores de Monterrey

School of Engineering and Sciences

Campus Toluca

Metabolic Flux Analysis of *Xanthophyllomyces dendrorhous* metabolism to understand the production of astaxanthin

A thesis presented by

by

Victor Ignacio Martínez Castro

Submitted to the School of Engineering and Sciences in partial fulfillment of the requirements for the degree of

Master of Science in Biotechnology

Estado de México, Toluca, June, 2020

Dedication

Mom I know you are watching over me from wherever you are, this is for you.

To Peter, thanks for your unconditional support no matter the distances you always have given me the courage to keep going.

To my life-partner, thanks for your unconditional love support and patience when everything was going sideways.

To my father, thanks for your support and love through this times.

To PhD. Rodrigo Balam Muñoz Soto, for leaving in me the passion for science and investigation, I hope this work could make you proud.

To my friends who believed in me and give me those words of encouragement when most I need them.

Acknowledgements

First of all, I would like to thank my supervisors at Tecnológico de Monterrey in CEM, PhD. Carlos E. Gómez Sánchez for his enormous patience, excellent guidance and his deeply interest in my formation as a researcher throughout the years. In Puebla PhD. Marco A. Mata Gómez, for his confidence and commitment to this project without his contributions this would not be possible.

I would like to express my acknowledgement to the Tecnológico de Monterrey, who provided support on tuition, and CONACyT who provided the funding for this work and for the grant No. 001550 which provided economical support. I would also like to express my sincere gratitude to MOI Paulina Ingelmo Díaz for providing me with equipment and expertise, vital for the completion of my work.

Many thanks to MM SCM Héctor Adiel Flores Nestor the great advices given to improve the project.

Last, but not least, I would like to thank my mother and life-partner for standing by me and encouraging me through this time.

Abstract

Carotenoid production by microorganisms, contrary to chemical synthesis, could fulfill the increasing demand for human consumption. The yeast *X. drendrorhous* is one of the most promising and economically attractive microorganisms for industrial production of astaxanthin. The metabolic pathway through which this yeast synthesize this valuable carotenoid is known. However, the complex mechanisms that are involved in the process, the distribution of the metabolic fluxes and the rates at which the pathways work, remain unknown. Several studies have provided different approaches to manipulate and improve carotenoid production in *X. dendrorhous* from classical mutagenesis to genetic engineering of the complete pathway covering improved precursor supply for carotenogenesis, enhanced metabolite flow into the pathway, and manipulating the relation C/N in the culture medium. However, it has not been reported quantitatively how nutrients, from the central metabolism and other pathways, converge in the carotenoids biosynthesis. In this study, the metabolism of *X. dendrorhous* growing in a continuous culture, under two ammonia conditions, Limited (L) and Non-limited (NL). The metabolic flux analysis (MFA) allowed to understand the distribution the intracellular fluxes along the different metabolic pathways evaluated, but most important, it elucidated that by limiting the ammonia assimilation flux(L= 0.002 $\pm$ 1.1 E-05; NL= 0.004 $\pm$ 4.3 E-05; g/g_{cell} h), a promotion of the astaxanthin formation flux was obtained (L= 86.4 $\pm$ 0.6; NL= 0; ug/g_{cell} h). This first approach will help to set a deeper study in order to understand the metabolic pathways that regulate the flux towards the astanxanthin biosynthesis.

List of Figures

List of Tables

Contents

1 Introduction

The carotenoid astaxanthin is a 3,3'-dihydroxylated and 4,4'-diketolated derivative of β-carotene (3,3'-dihydroxy- β, β',-carotene-4,4'-dione). It exists in three stereoisomers: (3S,3'S), (3R,3'R) (enantiomers) and (3R,3′S) (meso form) (Fig. 1). In nature, it is ingested by marine organism such as salmon, trout, shrimp and lobster, subsequently leading to the prominent colour of the flesh and shell, respectively [15]. This carotenoid has a broad application in aquaculture, cosmetic, food and pharmaceutical industries, and it was expected that by 2019 the global market value will reach nearly 1.8 billion USD. Nowadays, Chemical synthesis still is the method of choice for its production despite the high cost, and unfavourable environmental impact [8]. However, it cannot full-fill the market demand as a dietary supplement due to the lack of evidence regarding its safety for use as a human nutraceutical supplement. Moreover, it has been demonstrated that natural astaxanthin is 20 times stronger than synthetic in free radical elimination [4], meaning that the natural astaxanthin has better antioxidant properties than the synthetic. Several microorganisms are able to biosynthesis this carotenoid. The micro-algae *Haematococcus. pluvialis* and the red pigmented red yeast *Xanthophyllomyces dendrorhous*, also known as *Phaffia rhodozyma*, are the most promising microorganisms for commercial biotechnological production of astaxanthin since they accumulate the highest levels of this carotenoid in nature.

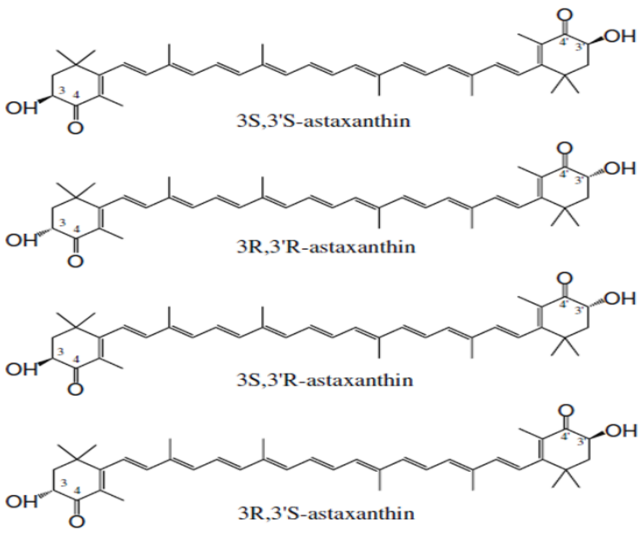

Figure 1: Configurational isomers of astaxathin.

Xanthophyllomyces dendrorhous is an heterobasidiomycete that synthesizes astaxanthin, for preventing the oxidative damage caused by oxygen species. Around 85% of the total carotenoid content of this yeast is astaxanthin. *X. dendrorhous* synthesize the (3R,3'R)-isomer, whereas most of the other carotenogenic microorganisms produce the (3S,3'S)- configuration [13]. However, it is important

to mention that the stereo-isomeric composition of astaxanthin does not affect the bio-availability in humans as measured in blood levels, which makes it an ideal nutraceutical[17]. In addition, the carotenoid synthesis pathway is well established, it starts transforming acetyl-CoA to isopentylpyrophosphate (IPP) via mevalonate pathway. Subsequently, eight molecules of IPP are condensed to form phytoene, which in turn is metabolized via four dehydrogenation and two cyclic reactions resulting in β-carotene. However, it has been reported that *X. denrorhous* can diverge from the dicyclic to a monocyclic pathway in three different ways transforming neurosporene, lycopene or γ/carotene into β-zeacarotene, 3,4-didehydrolycopene or torulene,respectively, instead of being metabolized intoβ-carotene [11]. As illustrated in Figure 2 any of these will result in the formation of derivates of torulene [13]. This could be a deviation of nutrients that could be used towards astaxanthin biosynthesis.

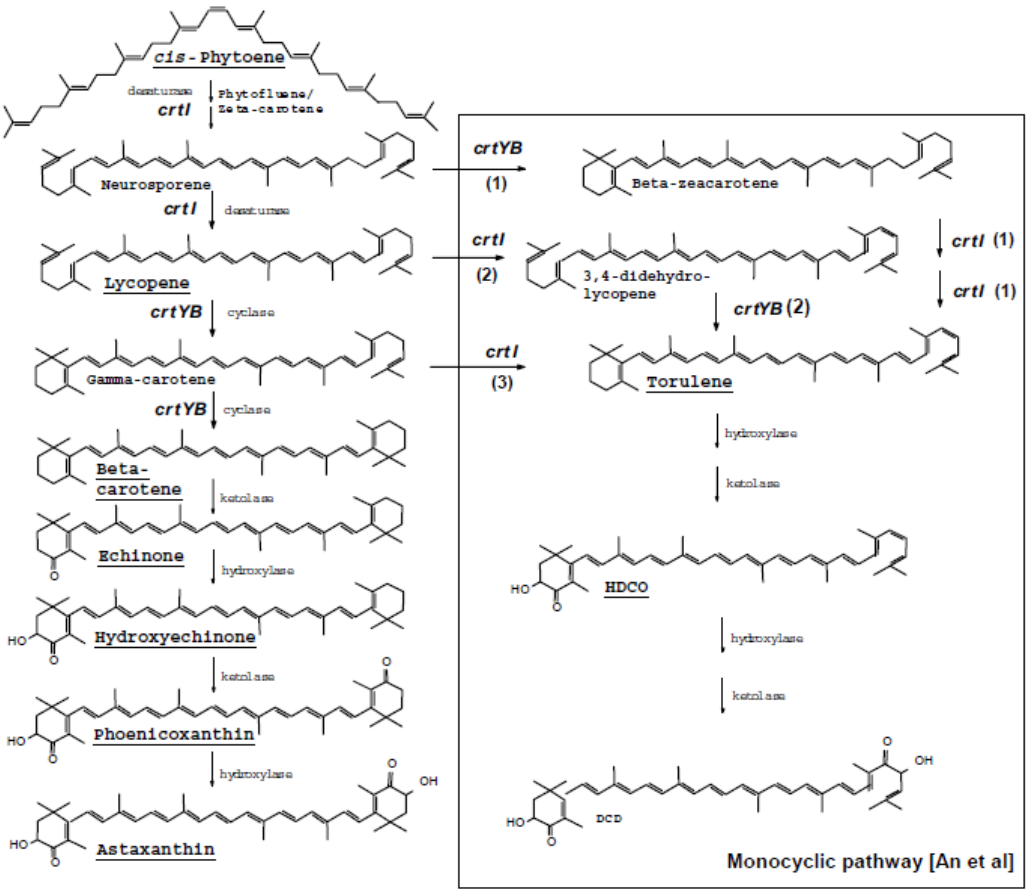

Figure 2: Dicyclic [1] and monocyclic (boxed area) [11] carotenogenic pathways in *X. dendrorhous*. Nomenclature: HDCO; 3-hydroxy-3P,4P-didehydro-L,i-carotene-4-one. DCD; 3,3P-dihydroxy-L,i-carotene-4,4P-dione. The numbers in the boxed area (1), (2) and (3), indicate the three potential routes to torulene.

Moreover, the genome of *X. dendrorhous* has been recently fully sequenced and published [22], allowing the elucidation of the genes involved in the synthesis of ergosterol, astaxanthin and fatty acids, which provides valuable tools for the metabolic engineering of the pathway. The three metabolites mention before use acetyl-CoA (Ac.CoA) as precursor, and in the case of astaxanthin and ergosterol, both share farnesyl pyrophosphate (FPP) as basic precursor, for this reason the genes involved in their synthesis could be targeted for modification in order to promote the formation of either one of them. Genetic engineering of enzymes involved in astaxanthin synthesis has been explored with aim of increasing the production of this molecule [27].

Since the early 2000′s there has been an increasing interest in the production of astaxanthin using *X. dendrorhous*. Many research efforts have been made for improving the yields of astaxanthin production. One approach has been random mutagenesis of wild strains and a selection process for the higher carotenoid contents result as an easy way to obtain new mutant strains, capable of having higher yield of astaxanthin production. Several chemical mutagenesis treatments with low concentrations of nitrosoguanidine or ultraviolet light exposure have been used for obtaining carotenoid hyper-producing strains. Nonetheless, genetic instability as well as the reduction in growth rate, and/or biomass yield is a major drawback for using these carotenoid hyper-producing strains for commercial exploitation. In addition, genetic engineering is performed with no previous knowledge of the key control points that regulates the synthesis of astaxanthin, which results in a time-consuming task. What′s more, it is not possible to secure that secondary mutations won′t affect the physiology, viability or metabolic capacity of the cell [26]. A more specific approach to avoid the latter, has been the targeted genetic modifications of the pathway. The elucidation of the carotenoid synthetic pathways at a genomic level allowed to have an increment in the carotenoid production yield with higher conservation of central functions [21]. Combination of classical mutagenesis with genetic pathway engineering has proven to be very effective to develop an extremely high astaxanthin accumulation in *X. dendrorhous* up to, 9.7 mg/g, compared to a wild-type strain that reaches up to 0.5 mg/g [25][26].

Another approach is the optimization of the culture media and culture conditions, including the addition of specific nutrients, optimization of parameters such as concentration of carbon and nitrogen sources, oxygen, temperature, and pH [13]. However, it is important to have in mind that *X. dendrorhous* exhibits two effects that have negative impact on the biomass and astaxanthin yields since this produces fermentation metabolites such as ethanol and acetate. Pasteur′s effect is present, having normal glucose concentration and aerobic conditions. On the other hand, when aerobic condition and high-glucose concentration are present the Crab-tree effect [28]. According to Koyunoglu Pasteur′s effect is defined as an inhibitory effect in the fermentative pathway due to oxigenic conditions and Crab-tree effect is the inhibition of respiration due to high concentrations of glucose [3].

Moreover, a high relation between the carbon and nitrogen source, C/N, supplied to *X. dendrorhous* cultures, has been related to an accumulation of carotenoids, however, why and how it affects the

accumulation of carotenoids remains unclear [20]. In addition, it has been reported that in oleaginous microorganism lipid accumulation is triggered when the cells exhaust the nitrogen source of the medium, but glucose is still being assimilated. In consequence, the cell supplies nitrogen by the deamination of AMP. The depletion of the AMP concentration leads to the inactivation of the mitochondrial isocitrate dehydrogenase, IDHC, only in oleaginous microorganism is AMP-dependant. Subsequently, this triggers the citrate accumulation, which is transported to the cytosol where it is transformed into oxaloacetate and acetyl-CoA (AcCoA) by the enzyme ATP-citrate lyase (ACL). The presence of ACL has been studied in *X. dendrorhous* and correlated with carotenoid accumulation, nonetheless, the activity of this enzyme was not dependant on limitation of ammonia, according to what they have reported [6]. It is important to emphasize that the basic formation unit of lipid and carotenoids is the AcCoA [10]. In this sense, we have hypotesized that under limited nitrogen conditions, *X. dendrorhous* will deviate the route towards acetyl-CoA accumulation, thus resulting in a promotion of the production of astaxanthin.

Finally, latest studies have been able to reveal the central metabolism of *Phaffya rhodozyma* when growing under steady-state conditions using a chemostat, in other words, the concentration of any chemical specie inside the culture vessel did not change through time. The obtained results allowed to create a metabolic flux model of its central metabolism. These results have helped to identify that the central carbon metabolism is more similar to a metabolism of a filamentous fungus than that to of a *S. cerevisiae* [7].

In spite of the enormous advances that have already been done towards the understanding and optimization of astaxanthin production in *X. dendrorhous*, still remains unclear which strategy is an optimal approach to study the mechanisms involved in carotenoid synthesis, an alternative strategy is to study the metabolism through the Metabolic Flux Analysis (MFA). The MFA is the reaction network stoichiometries describing how substrates are converted to metabolic products and biomass constituents. Analysis can be done by mathematically modelling the key reactions involved in the production of certain metabolite. The determination of intracellular metabolic fluxes may be based either on an equal number of metabolite balances or on a greater or smaller number of such balances, depending on the number of available measurements, whereas with more measurements available the validity of the process can be rigorously assessed through mathematical analysis. This analysis of the metabolism allow to visualize the cell from another perspective, in other words, can lead to an enhancement of cellular function and metabolism by having a broader perspective about the behaviour of the whole metabolic system [12]. It is important to mention that a metabolic network model of the central metabolism of *X. dendrorhous* has already been proposed and allowing to elucidate the distribution of carbon in glycolysis, penthose phosphate pathway and the Tri-Carboxylic acid cycle [7].

In this work, it was proposed to analyze the influence of ammonia assimilation in the formation

of astaxanthin by *X. dendrorhous* through Metabolic Flux Analysis (MFA) of the central metabolism of this yeast and its alternative pathways that converge in the synthesis of astaxanthin. Experimental measurements of key metabolites during the growth of the yeast under steady-state conditions in a chemostat bioreactor were fed into a mathematical model to calculate intracellular metabolic fluxes.

1.1 Hypothesis

The limitation of the ammonium assimilation flux lead to an arrest of the krebs cycle, accumulating citrate, which is transported to cytosol and converted to acetyl-CoA, the first precursor for synthesis of lipids and carotenoids. In this sense, the limitation of ammonium assimilation rate will promote the formation flux of astaxanthin.
The research questions which shall be answered in this project are the following:

- Which are the key precursors for the synthesis of astaxanthin and their intracellular fluxes?
- How will be defined the limitation of assimilation of ammonium?
- How can it be defined which metabolic fluxes are relevant?
- How to defined which fluxes are going to be measurable and calculable?

1.2 General objective

The overall objective of this research project is to demonstrate that the limitation of ammonia assimilation flux promotes the formation flux of astaxanthin.

In order to achieve this objective, the short-term objectives that must be attained are:

- Standardization of a chemical defined medium. This allows to make a specific and quantifiable stoichiometric balances because the carbon, nitrogen and trace element sources are well identified.
- Standardization of a continuous culture based on the chemostat theory.
- Building the Metabolic Network, starting with the identification of the sets of reactions directly and indirectly involved on the synthesis of astaxathin. Consequently set the balance equation of the relevant metabolites.
- Develop and solve the Metabolic Network Model in Wolfram Mathematica v11.3. Translate the Metabolic network of the relevant metabolites into a linearly, homogeneous and independent, system of equations and solving it for obtaining an estimation of the intracellular fluxes of the relevant metabolites under limited and non limited ammonium conditions.

2 Background

2.1 Metabolic Engineering

As it is with all traditional fields of engineering, metabolic engineering encloses the two dimensions of analysis and synthesis. Due to the emerging of metabolic engineering was simultaneously with DNA recombination technology, at the early stages, the investigation was mainly focused on the synthetic side of this field; expression of new genes in various host cells, amplification of endogenous enzymes, deletion of genes or modulation of enzymatic activity, transcriptional or enzymatic deregulation, etc. As such, metabolic engineering was, to a significant extent, the technological manifestation of applied molecular biology with very little engineering content [12]. It is important to mention that all the Bioprocess considerations do not qualify as metabolic engineering.

A more engineering form to approach this matter can be found in the analytical dimension. First, it is crucial to identify the main parameters that define the physiological state. Secondly and more important, how can this information be utilized to elucidate the control architecture of a metabolic network and then propose rational targets for modification to achieve certain objective? For example improving the production yield of a valuable metabolite. Furthermore, after knowing the key points that control the metabolic network; is it possible to assess the true biochemical impact of such genetic and enzymatic modifications in order to design the next round of pathway modifications and so on until the goal is attained? These are some areas the analytical dimension would address. On the other hand, a novel aspect regarding the synthetic dimension is, instead of only put special attention to a specific individual reaction, staring to a picturing, a large image, which focuses on complete biochemical reactions networks, and address its synthesis and thermodynamic feasibility, as well as pathway flux and its control. In other words, considering a metabolic network one can lead to an enhancement of cellular function and metabolism by having a broader perspective about the behaviour of the whole system. Now it can be defined Metabolic engineering as, the combination of analytical methods to quantify fluxes and their control with molecular biological techniques to implement suggested genetic modifications [12]. It is important to highlight that not only can be suggested genetic modifications but also environmental, such as, pulses of certain nutrient that stimulates the activation of certain pathway.

The metabolic fluxes play a fundamental role in the cell physiology because they provide a measure of how nutrients diverge or converge in various pathways of cellular functions and metabolic processes. Therefore accurate quantification of the magnitude of pathway fluxes *in vivo* is an important goal of metabolic engineering, especially in the context of metabolite production, where the main target is to consume as much substrate as possible and transform it into useful products [12].

2.1.1 Metabolic Flux Analysis

A powerful methodology for the calculation of metabolic fluxes is the metabolic flux analysis (MFA). Whereby intracellular fluxes are calculated by using a stoichiometric model for the major intracellular reactions and applying mass balances to intracellular metabolites. A set of well-studied and selected substrates of uptake rates and metabolites secretion rates are measured to used them as inputs for mathematical models that estimate intracellular fluxes. The final outcome of these calculations is a metabolic flux map showing a diagram of the biochemical reactions described in a steady state fashion. An example of a metabolic map is illustrated in figure (3).

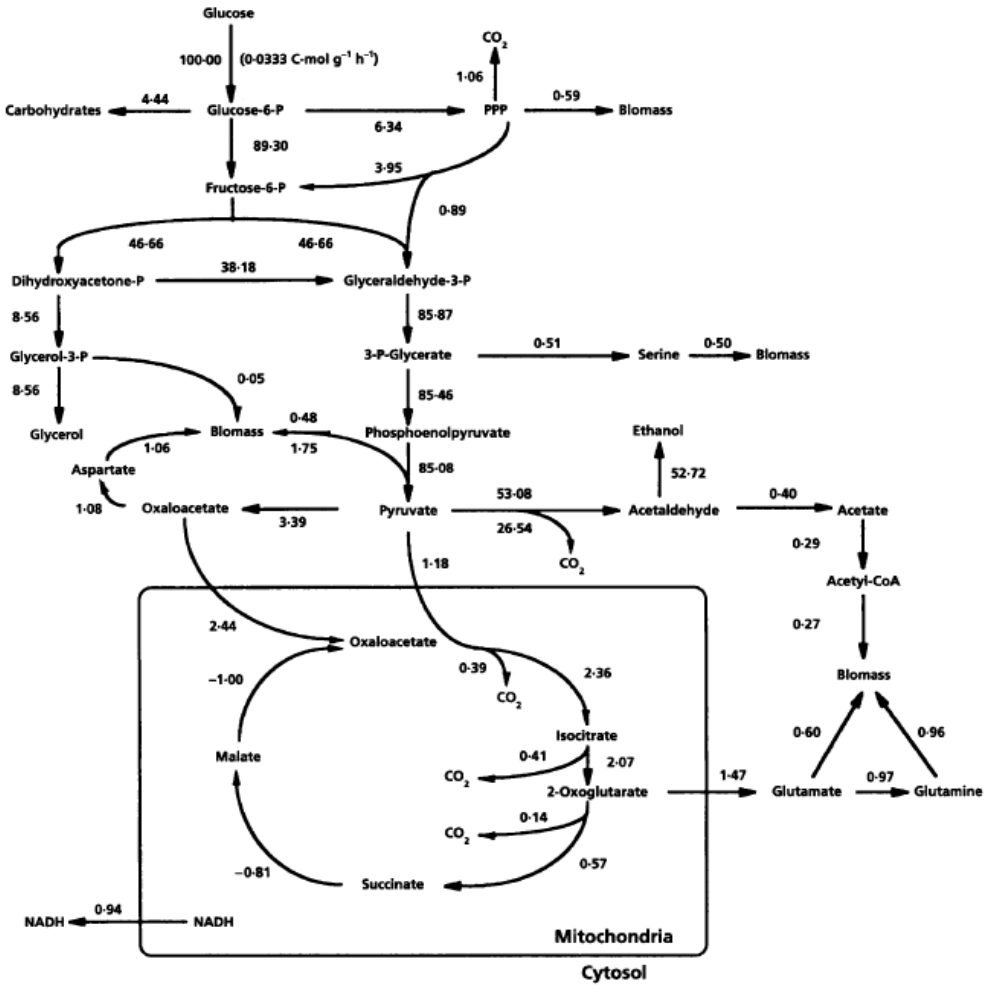

Figure 3: Fluxes through different common metabolic pathways of *Saccharomyces cerevisiae* under anaerobic growth conditions. The fluxes were calculated using the stoichiometric model established by Nissen [19].

One particular aspect of MFA is that the stoichiometric determination of intracellular metabolic fluxes may be based either on an equal number of metabolite balances or on a greater or smaller

number of such balances, depending on the number of available measurements. In first case there is no redundancy, whereas the more experimental measurements are included in the model, the more validity of the process can be rigorously assessed. On the other hand, in case of having fewer measurements available, fewer than the system degrees of freedom, therefore, an infinite number of solutions exist for the network fluxes[12]. In these cases it is necessary follow other strategy to find a solution to the system, it can be done by making a simplification analysis of the stoichiometric model in order to obtain a number degrees of freedom that match with the available measurements or by declaring constraints in order to complete the missing measurements.

The starting point of MFA is the stoichiometry of the reaction network describing how substrates are converted into metabolic products and biomass constituents. If there are J reactions considered and they proceed via K pathway metabolites, the mass balances are given by,

$$\frac{\mathrm{d}\mathbb{X}_{met}}{\mathrm{d}t} = r_{met} - \mu\mathbb{X}_{met} \tag{1}$$

where X_{met} is the vector con concentration for the intracellular metabolites, and r_{met} is the vector containing the net rates of formation of the intracellular metabolites in the J reactions [12], and μ the specific growth rate of the study organism. It is generally accepted that inside the cell the concentrations of the different metabolite pools rapidly adjust to new levels, even after large perturbations in the environment experienced by the cells when exposed to different environments. As a result it can be assumed a pseudo-steady state, in other words, there is no metabolite accumulation, and therefore $dX_{met}/dt = 0$

$$0 = r_{met} - \mu\mathbb{X}_{met} \tag{2}$$

The first term r_{met} on equation 2, express the sum of fluxes leading into and out of a pathway metabolite, while the second term, physiologically speaking, refers to the dilution effect of metabolite pool due to biomass growth [12]. Because the intracellular level of most pathway metabolites is very low, the dilution effect is generally small, especially compared with other fluxes affecting the same metabolite, consequently the dilution term μX_{met} could be neglected leaving a simpler balance

$$0 = r_{met,i} = \sum_{j=1}^{J} \alpha_{ij} r_j \tag{3}$$

where the specific rate vector r_{met} contains the net rates and the sum, $\sum_{j=1}^{J} \alpha_{ij} r_j$, contains the sum of the products between the stoichiometric coefficient of the ith metabolite in the jth reaction, α_{ij}, and the net rate of the jth reaction, r_j, in other words equation 3 state a linear system of equations where the net formation of i metabolites, contained in $\mathrm{r}_{met,i}$, is equal to the formation and consumption of this metabolites in all the J reactions.

2.2 Metabolic Pathways involved in Astaxanthin Production

The series of bio-reactions that are involved in the synthesis of astaxanthin in *X. dendrorhous* will be stated in the following 8 blocks of metabolic pathways:

- Glycolysis
- Tri Carbolxylic Acid Cycle
- Pentose Phosphate
- Mevalonate Pathway
- Carotenoid biosynthesis
- Ammonia assimilation
- Oxidative Phosphorylation
- Structural Carbohydrate Synthesis

In addition, a metabolic map of *X. dendrorhous* was constructed using these 8 metabolic block and is shown in Figure 4. For more information on the stoichiometry of every reaction involved see appendix B. It is important to mention that the information of each metabolic pathway was from Kyoto Encyclopedia of Genes and Genomes (KEGG) and MetaCyc Metabolic Pathways databases.

2.2.1 Glycolysis

Glycolysis is the total sum of all biochemical reactions by which glucose is converted into pyruvate. There are three main pathways (1) the $Embden\text{-}Meyerhof\text{-}Parnas$ (EMP), (2) the $pentosephospate$ (PP) and (3) the $Entner\text{-}Doudoroff$. Two of them are present in *X. dendrorhous*, that are, the EMP and PP pathways [12]

In EMP pathway, the entering fructose-6-phosphate (F6P) is converted into 2 mol of pyruvate. Even that the conversion of F6P to fructose-1,6-biphosphate (F1,6P), requires free energy from ATP, there is still an overall gain of 3 mol of ATP per mole of glucose-6-phosphate (G6P). In the oxidation of glyceraldehyde-3-phosphate (G3P) to 1,3-biphosphoglycerate (G1,3P), NADH is produced. Hence the overall balanced stoichiometry reaction for the conversion of glucose to pyruvate is

$$2pyruvate + 2ATP + 2NADH + 2H_2O + 2H^+ - glucose - 2ADP - 2 - P - 2NAD^+ = 0 \quad (4)$$

2.2.2 Pentose Phosphate Pathway

In the PP pathway, before glucose enters the pathway it is needed to be phosphorylated in the C-6, being transformed in G6P. Then it is oxidized to 6-phosphogluconate (GLT6P), which is further

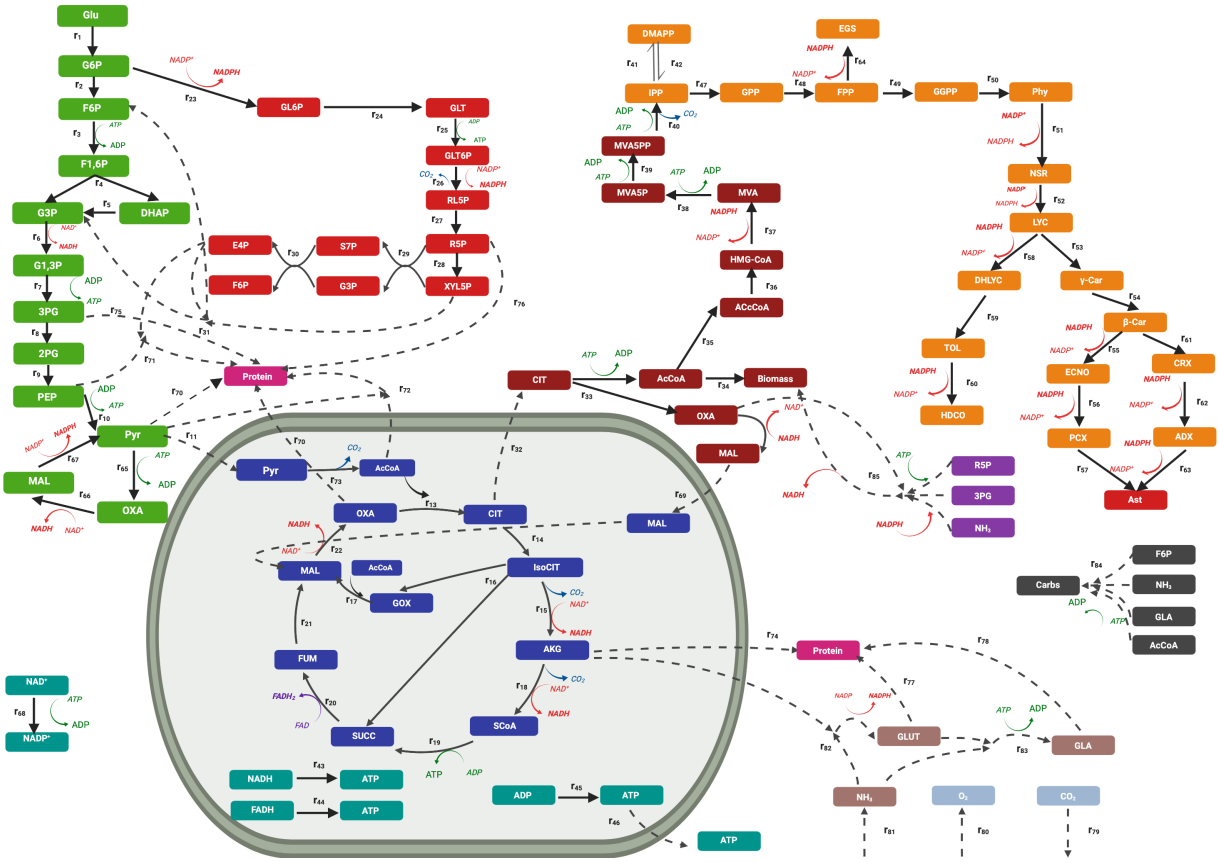

Figure 4: Proposed Metabolic Network of *Xanthophyllomyces dendrorhous*. The metabolic blocks are depicted with the following coding: Green, Glycolysis; Red, Pentose Phosphate Pathway; Blue, TCA/Krebs Cycle; Aqua, Oxidative Phosphorylation; Black, Carbohydrate synthesis; Purple, Nucleic Acid Synthesis; Brown, Ammonia Assimilation; Wine,Lipid Synthesis and Mevalonate Pathway; Orange, Carotenoid Synthesis; Pink, Protein Synthesis; Grey, CO_2 and O_2 transport. The white are is the cytosol and the mitochondria is the light grey area delimited with a bi-layer.

converted to ribulose-5-phosphate (RL5P) and carbon dioxide. In each reaction is formed 1 mol of NADPH per mole of G6P is formed. In following reactions, RL5P is converted into ribose-5-phosphate (R5P) or erythrose-4-phosphate (E4P), which both are precursors for amino acids and nucleotides. In a different sequence of reactions, RL5P may also be converted back to F6P and G3P, consequently re-entering the EMP pathway [12].

The overall stoichiometry depends on the extent of which carbon entering the PP pathway is recycled back into the EMP pathway to be oxidized into carbon dioxide or consumed for the formation of bio-synthetic precursors, such as five carbon sugars for ribonucleotide synthesis. For the latter, this pathway has been recognized to serve as oxidative as well as an anaplerotic function, each described by the following

- Anaplerotic function:

$$6R5P + 5ADP + 4H_2O - 5G6P - 5ATP = 0 \tag{5}$$

- oxidative function:

$$12NADPH + 12H^+ + 6CO_2 - G6P - 12NADP^+ - 7H_2O = 0 \tag{6}$$

2.2.3 Tri Carboxylic Acid Cycle (Krebs Cycle)

The first step is an oxidative decarboxylation of piruvate leading to formation of Acetyl-CoA. This reaction is catalyzed by a cluster of three enzymes, called PDC (Pyruvate Dehydrogenase Complex). Then Acetyl-CoA condensed with oxaloacetate to form citrate. Subsequently, citrate is converted to isocitrate. The next two reactions are oxidative decarboxylation, first, isocitrate is transformed to α-ketoglutarate, and subsequently, α-ketoglutarate is converted to succinyl-CoA. In the following reaction, succynil-CoA is hydrolyzed to succinate with liberation of Gibbs free energy due to the hydrolysis of CoA ester bond. In the next step succinate is dehydrogenated to fumarate. Here, due to the necessity of a strong oxidizing agent, FAD^+ is reduced to $FADH_2$. Then fumarate is converted to L- malate and the cycle's final step is the formation of oxaloacetate from L-malate.

The overall stoichiometry for the complete oxidation of pyruvate in the TCA cycle is

$$3CO_2 + GTP + 4NADH + FADH_2 + 4H^+ - pyruvate - 3H_2O - GDP - 4NAD^+ - FAD = 0 \tag{7}$$

2.2.4 Mevalonate Pathway

The biosynthesis of astaxanthin starts from Acetyl-CoA (AcCoA), which is transformed to HMG-CoA (hidroxy methylgrutaryl-CoA). Then HMG-CoA is reduced to Mevalonate (MVA). In the next two steps, mevalonate is phosphorylated twice resulting in PP-mevalonate. Finally, PP-mevalonate is decarboxylated to isopentyl-pyrophospphate (IPP) [21]. IPP is the general precursor of all carotenoids. The overall stoichiometry for the obataing 1 mol of IPP is

$$IPP + 2NADP^+ + 3ADP + CO_2 + 3CoA - 3AcCoA - 2NADPH - 3ATP = 0 \tag{8}$$

2.2.5 Carotenoid Synthesis Pathway

Initially a molecule of dymethylallylpyrophosphate pyrophosphate(DAMPP) and three molecules of IPP are combined to obtain geranylgeranyl pyrophosphate (GGPP) by means of the GGPP synthase. Secondly, two molecules of GGPP are coupled by the phytoene synthase to reach phytoene. The phytoene desaturase introduces four double bonds in the molecule of phytoene to to obtain lycopene.

Then, the lycopene cyclase converts one of the ψ acyclic ends of lycopene as β-ring to form γ-carotene. Subsequently, the other end of lycopene to transform into β-carotene. Xanthophylls bio-conversion in X. dendrorhous from β-carotene and γ includes the addition of two 4-keto groups in the molecule of β-carotene by the ketolase activity, and the inclusion of two 3-hydroxy groups by the hydroxylase activity. Both activities are presented in a single enzyme astaxanthin synthetase (Asy). The cytochrome P450 reductase is an Asy helper protein that provides with electrons for substrate oxygenation [2]. The existence of a monocyclic pathway has been also established leading to the formation of 3,3-dihydroxy-β, ψ-carotene-4,4$'$-dione (DCD) and 3-hydroxy-4-ketotorulene (HDCO) [11]. This meaning that instead of cycling both sides of the molecule as depicted in fig (1) it is cycling just one side, resulting in DCD and HDCO.

2.2.6 Ammonia Assimilation

Nitrogen assimilation is the first step in amino acids biosynthesis, where nitrogen in form of ammonia, is fixed and incorporated into a α-ketoglutarate to form L-glutamate, this reaction is catalyzed by NADP-dependant glutamate dehydrogenase. Subsequently, L-glutamate and a ammonia is fixed in order to synthesize L-glutamine by glutamine synthase. L-glutamine serves as an ammonia donor in the biosynthesis of several nitrogen-containing molecules [12].

2.2.7 Oxidative Phosphorylation

From the complete oxidation of pyruvate in the TCA cycle it is obtained 4 mol of NADH and 1 mol of FADH, under aerobic conditions the electrons of NADH and FADH are transferred to free oxygen through a chain of electron acceptors. These acceptors are located in the inner mitochondrial membrane. For eukaryotes, 3 and 2 mol of ATP is generated for each mole of NADH, and FADH, respectively. The overall stoichiometry is:

$$5ATP - ADP - NADH - FADH - 5O_2 = 0 \tag{9}$$

2.2.8 Structural Carbohydrate Synthesis

The reaction considered for the formation of structural carbohydrate is the formation of UDP-N-acetylglucosamine (UDP-NAG) which is the building block for chitin synthesis, which is a component of the cell membrane. In order to form 1 mole of UDP-NAG a mole of AcCoA, a fructose, and a L-glutamine, as amino donor, is incorporated.

2.3 Continuous Culture and Chemostat Theory

The continuous culture of microorganisms has an essential future as growth occurs under steady-state conditions, in other words, growth occurs at a constant rate and at a constant environment. Moreover, the culture conditions may be independently controlled by the experimenter [14]. In the

specific case of the Chemostat, the reactor is defined as a culture vessel in which the organism can be grown under suitable conditions. In addition, fresh and sterile growth medium is fed into the culture vessel at a steady flow rate (Fa) and simultaneously broth culture, carrying cells, emerges from the vessel at the same rate. This operation s of upmost importance to achieve and maintain steady-state conditions. In addtion, the contents of the vessel must be sufficiently well stirred to approximate to the ideal complete mixing, this mean when the media enter the vessel is instantaneously and uniformly dispersed throughout the vessel[14], as shown in (Fig. 5).

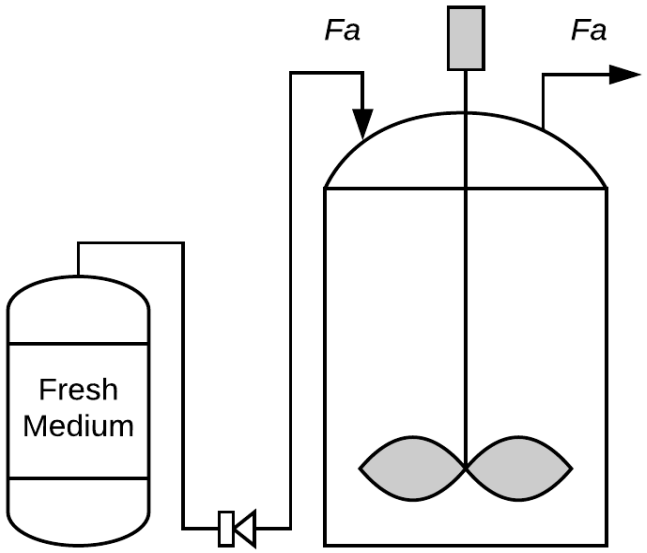

Figure 5: Schematic of a Chemostat. *Fa* stands the steady flow rate.

Before to start establishing the equations that describe the changes inside the culture vessel, first it is important to take some additional considerations to the Chemostat bioreactor, previously described.

- The culture medium that is being administrated has only one carbon source and at a determined concentration, Sa.
- The culture aeration is enough to supply the oxygen uptake of the microorganism to avoid a metabolic change from aerobic to anaerobic. This depends directly to the oxygen uptake rate of the microorganism.
- The supply of substrate is the sole growth-limiting factor.

Therefore, the variables to be controlled are the substrate concentration, Sa, and flow rate, Fa of the in-going medium. A complete theory that describes the effects on the specific growth rate, μ,

biomass concentration, x, and substrate concentration, S, is deeply explained in [14]. However, the basis will be well explained in the following part. To establish the total change of biomass, first, the rate of accumulation that will be given by the specific growth rate, μ, of the microorganism, should be considered. However, at the same time, biomass, X, it is being washed out at a flow rate, Fa. As result, the net change is given by the following balance equation:

Net change of biomass $[XV]$ = growth rate - exit flow rate

$$\frac{\mathrm{d}(XV)}{\mathrm{d}t} = \mu(XV) - FaX \tag{10}$$

If its divided by the volume at it will be operating the reactor , V, the equation (10) turns into a very important relation between the flow rate, Fa, and the operation volume, V:

$$\frac{\mathrm{d}X}{\mathrm{d}t} = \mu X - \frac{Fa}{V}X \tag{11}$$

The relation Fa/V represents the fraction of the operation volume that is being re changed per hour, or also called the dilution rate, D. Then substituting D in equation (11):

$$\frac{\mathrm{d}X}{\mathrm{d}t} = \mu X - DX \tag{12}$$

Hence if $\mu > D$, dX/dt is positive as result, the concentration of microorganism will increase. On the contrary, if $D > \mu$, dX/dt turns negative this mean that the microorganism are being wash out faster than its growth therefore, the concentration will decrease, eventually to zero. However, when $\mu = D$, there is no change in the concentration of biomass, in other words the concentration of biomass, X, is constant. Nonetheless, equation (**??**) by itself gives no information on what dilution rates makes a steady state possible. In order to do so, first it has to be established how dilution rates affects the concentration of substrate inside of the culture vessel, reminding that μ depends on the substrate, has to be established[14].

For understanding the net change of concentration of substrate it should be stated that substrate is entering the reactor at a concentration ,Sa , is being consumed by a the microorganism and washed out at a concentration, s. Establishing the balance:

Net Change of concentration of substrate [s] = inflow rate - washed out rate - consumption rate

$$\frac{\mathrm{d}[s]}{\mathrm{d}t} = DSa - Ds - \frac{\mu X}{Y_{x/s}} \tag{13}$$

where the inflow and washed out rates are given by the products of the dilution rate , D, times the concentration of the feeding substrate, Sa and s, respectively. The consumption rate is given by the relation between the product of the specific growth rate, μ times the concentration of biomass, x, and

the biomass yield, $Y_{x/s}$.

For understanding the the net change of the concentration of a product, P, it should be stated the following, product is being formed at a certain rate and is being washed out at a ,P, concentration. However, before establishing the balance, first it will be defined the formation rate of a product as follows,

$$\frac{\mathrm{d}[P]}{\mathrm{d}t} = (\alpha\mu + \beta)X \tag{14}$$

the equation (14) was first proposed by Luedeking-Piret [18], which state that the formation of a product is associated both to growth being the term, $\alpha\mu$ and the concentration of cells represented by, β. Stating the balance as,

Net Change of concentration of substrate [P] = product formation rate - washed out rate

$$\frac{\mathrm{d}[P]}{\mathrm{d}t} = (\alpha\mu + \beta)X - DP \tag{15}$$

The balances stated in equations (12), (13), and (15), are the basis to calculate the fluxes of biomass, q_X, substrate, q_s, and product, q_P. First these 3 equations are divided by the biomass concentration, X, resulting in,

$$\frac{\frac{\mathrm{d}[X]}{\mathrm{d}t}}{X} = \mu - D \tag{16}$$

$$\frac{\frac{\mathrm{d}[s]}{\mathrm{d}t}}{X} = (Sa - s)DX - \frac{\mu}{Y_{x/s}} \tag{17}$$

$$\frac{\frac{\mathrm{d}[P]}{\mathrm{d}t}}{X} = (\alpha\mu + \beta) - \frac{DP}{X} \tag{18}$$

Second, we defined and the fluxes, q_X, q_s, and q_P as the relation between the net change, $\frac{dW}{dt}$, and biomass concentration, X. Being W either X, s, or P. Finally substituting the fluxes in equations and assuming steady state condition, (16), (17), and (18) and assuming steady state condition, the result is the following,

$$\mu = D \tag{19}$$

$$q_s = (Sa - s)DX \tag{20}$$

$$q_P = \frac{DP}{X} \tag{21}$$

the equations (19), (20), and (21) state how to obtain the fluxes from experimental data of concentration of biomass, X, substrate, s, and product, P, obtained under steady state conditions.

3 Methodology

In this section the different procedures were followed in order to probe the hypothesis, previously stated, are explained. It is important to mention that each determination was made by triplicate (n=3), the average value of each sample is reported with a confidence interval (CI) calculated with a t-student distribution with a level of significance 5% ($p<0.05$).

3.1 Microorganism and conservation of the strain

For the development of this thesis project, the strain *Xanthophyllomyces dendrorhous* CECT-1690 was used. The yeast was grown on YM agar plates by streak plate method once a month to preserve it. The Petri dishes were incubated at 22°C for 72 h. Then they were stored at 4°C for a month until used.

3.2 Culture Medium Preparation

Tables 1 and 2 illustrate the chemical composition of the defined medium and the YM (Yeast-Malt) medium, respectively. All the components were dissolved in de-ionized water and then sterilized in the autoclave for 15 min and at 121°C. Before sterilization, pH is adjusted at 5.5 with NaOH 1 M and HCL 1 M. It is important to highlight that the vitamin solution must be added after sterilization, due to the thermolabile nature of the vitamins. Thus they were sterilized by filtration, using a membrane of 0.22μm.

Table 1: Chemical composition of the Defined Mineral medium for *X. dendrorhous*. * For more information go check subsection 6.3 Solutions Preparation, Tables 3 and 5

Compound	**Concentration (g/L)**
Dextrose	10
Ammonium Sulphate	5
Monobasic Potassium Phosphate	1.5
Heptahydrate Magnesium Sulphate	1.5
Calcium Chloride	0.6
Vitamin Solution* mL/L	0.2
Mineral Solution* mL/L	0.1

Table 2: Composition of the YM medium for *X. dendrorhous*.

Compound	Concentration (g/L)
Dextrose	10
Bacteriological Agar	10
Yeast Extract	5
Malt Extract	3
Casein Peptone	3

3.3 Mineral and Vitamin solution preparation

The following mineral solution described in Table 3 is prepared in a volumetric flask adding the compound from the least soluble to the most soluble. At the moment any compound stop solubilizing, HCL (36% w/w) was gradually added. During previous tests of the solutions preparation, showed that the approximate ratio of water and HCl preparing a 100 mL of solution is 1:1. The constants of solubility for each compound are shown in Table 4. In the case of the vitamin solution, only biotin is prepared apart due to is low solubility in water. 1M NaOH was added to increase its solubility. Meanwhile, the other vitamins are prepared in the same pool adding from the least to the most soluble. The Tables 5 and 6 show the composition of the vitamin solution and the solubility constants for each vitamin, respectively. Finally, both vitamin solutions (Biotin and Vitamin Pool) are sterilized by filtration using a membrane with a pore diameter of 0.22 μm under aseptic conditions. All solutions were stored at 4 °C, flasks were wrapped with aluminum foil to avoid mineral photo-degradation.

Table 3: Composition of the Mineral solution.

Compound	Concentration (g/L)
Sodium Molybdate	20
Pentahydrated Copper Sulfate	60
Hydrated Manganese Sulfate	30
Heptahydrated Zinc Sulfate	80
Hexahydrated Iron Chloride	75

Table 4: Saturation Constants for each compound of the mineral solution.

Compound	Solubility in water (g/100ml)
Sodium Molybdate	92
Pentahydrated Copper Sulfate	70
Hydrated Manganese Sulfate	62
Heptahydrated Zinc Sulfate	20.3
Hexahydrated Iron Chloride	9.6

Table 5: Composition of the Vitamin solution.

Compound	Concentration (g/L)
Biotin	0.8
Myo-Inositol	50
HCl-Thiamin	50
HCl-Pyridoxine	22.5

Table 6: Saturation Constants for each compound of the vitamin solution.

Compound	Solubility in water (g/100ml)
Biotin	0.02
Myo-Inositol	5
HCl-Thiamin	5
HCl-Pyridoxine	Highly soluble

3.4 Continuous Culture Conditions

The system used to established the continuous culture was composed by the following elements. A New Brunswick BioFlo ®/CelliGen ® 115 bioreactor was used as the culture vessel operated at 3 L. The air flow rate into the bioreactor was fixed at 0.5 vvm (1.5 SLPM). The temperature of the bioreactor was kept at 22°C and pH at 5.5 (with 0.5 M HCL and 0.5 M NaOH). DO (Dissolved Oxygen) was controlled at 20 ± 2 % air saturation by varying the agitation from 200-900 rpm, which is significantly different from the critical DO of this yeast, which is 10% [28]. The sterile defined medium (Table 1) was fed into the culture vessel once reached 40 hours of cultivation. A BioFlo® 415 bioreactor was used to formulate 15 L of the defined medium and sterilized it in place at 121 °C for 15 min. Up to 2L approximately were lost due to evaporation during the sterilization cycle. Once the sterile defined medium cooled down at a 30 °C, the vitamin and mineral solutions were added. Finally, the 15 L reservoir was connected to one of the inlets of the culture vessel with a silicon hose (bio-pharmaceutical grade), previously sterilized. The sterile medium was pumped with an peristaltic pump integrated into the module of the BioFlo ®/CelliGen ® 115 bioreactor. The culture broth was

flowing out at the same rate as the sterile medium was being fed, from the sampler tube of the culture vessel into two 2L reservoirs, previously sterilized in an autoclave at 121 °C for 15 min. The whole system is depicted in Figure 6. Two experiments were carried out at two different concentrations of glucose (without NH_3-limitation 5 g/L, with NH_3-limitation 10 g/L) and ammonium sulfate (without NH_3-limitation 1 g/L, with NH_3-limitation 0.5 g/L), the other components remain the same as stated in Table 1. The medium was pumped at a different flow rate in each experiment (without NH_3-limitation 108 $\pm$ 3 mL/h, with NH_3-limitation 50.4 $\pm$ 1 mL/h). Each experiment was monitored by taking a 15 mL sample, with a sterile 15 mL-conical tube (Falcon®), every 4 hours until the feeding started, except when from 18:00h - 9:00h. From this point until, and the steady-state condition was achieved, the samples were taken from the outlet of the sampler tube, putting the conical tube in an ice bath under aseptic conditions. Samples were taken in the morning (9:00 h) and before the Lab Centre closed (17:00 h). Each sample was centrifuged in an eppendorf ® centrifuge 5810r at 4000 rpm and 4 °C for 15 min. The supernatant was decanted in a clean conical tube and stored at 4 °C for further analysis of glucose and ammonia concentrations. The biomass pellet was re-suspended in 15 mL of filtered distilled water, and centrifuged twice in order to wash any remain of culture broth. The biomass suspension was stored at 4 °C for further analysis such as quantification of biomass on a dried basis, carotenoids, astaxanthin, and total carbohydrates content.

Figure 6: Bioreactor system (BioFlo Celli/Gen 115 New Brunswick Bioreactor) used to established the continuous culture of *Xanthophyllomyces dendrorhous*

3.5 Quantification of Biomass, Astaxanthin and Carotenoids Contents

In order to measure biomass, yeast cell were separated from the culture broth, obtained from the samples. Centrifuging, at 4000 rpm for 12 min and at 4 °C. Biomass pellets were rinsed twice with distilled water in order to remove any remains of broth and re-suspended in the same volume of distilled water that had the sample. From here, the sample is divided in two parts. The first part was used for quantifying by gravimetry. In order to do this, 2 mL of the washed-cell solution were placed in an aluminum tray, previously weighted and labeled, and then dried for 24h at 105 °C. Finally, the aluminum trays containing the dried biomass were kept at constant weight in a desiccator and weighted in an analytical balance. was calculated as the difference between the weight of the sole aluminum tray and the tray containing the dried biomass. the dried weight, dw, was calculated as the difference between the weight of the sole aluminum tray and the tray containing the dried biomass.

The second part of the cell solution, was used for extraction and quantification of carotenoids. First, for the extraction of the carotenoids was used a combination of the methods stated by Sedmak [23]. This consisted in, placing 0.1 mL of 0.5 mm diameter glass beads, measured with an conic tube of 1.5 mL, in the tube with 1 mL of cells solution at no more than 0.5g/L of biomass. Then 0.5 mL DMSO (dimethyl sulfoxide), previously heated at 55 °C, was added to the cell suspension and it was mixed with a vortex for 30 seconds to promote cell disruption. Subsequently, 1 mL of hexane:ethyl acetate 1:1 (v/v) HPLC grade was added to each tube and they were mixed for 50 seconds in vortex. Finally, the contents of astaxanthin was determined by HPLC (Modular High Performance Prominence, Shimadzu) with a reversed-phase Phenomenex C18 column (5 μm, 150x4.6 mm). The mobile phase consisted of acetonitrile (A) and methanol (B) pumped at 0.5 ml/min in a gradient scheme: 10% B from 0 to 6 min, 10–30% B linear gradient from 6 to 13 min, and 30-10% B from 13-15min [15]. The astaxanthin was monitored with a UV/vis himadzu SPD-20A detector at 478 nm and confirmed and quantified by chromatography with astaxanthin standard (Merck, Product No. 41659) (astaxanthin at 13.0 min elution time). The quantification of total carotenoids, including astaxanthin and other carotenoids, was determined by spectrophotometry at 480 nm and using an extinction coefficient of 2150 cm2/g [23].

3.6 Quantification of Dextrose

The quantification of dextrose was performed by the method developed by Miller using DNS (3,5-dinitrosalycilic acid). It allows to measure any reducing sugar, that is any monosaccharide with an aldehyde or keto group. Dextrose (0.1-1mg/mL) was used as standard to prepare a calibration (Table 9) to measure glucose concentration in the cell-free broth.

3.7 Quantification of Total content of Carbohydrates

The quantification of total carbohydrates was carried out according the phenol-sulfuric acid method [24]. It is a simple and rapid colorimetric method that detect virtually all classes of carbohydrates

(mono-, di-, oligo- and polysaccharides). Even though this method detects almost all carbohydrates, the absorptivity varies with each carbohydrate. In the cases where there are more than one type of carbohydrate in a sample, the results must be expressed in terms of one carbohydrate, the experimenter may choose which. Before beginning the reaction, the following reagents must be prepared as follows.

- Solution A: Glucose Standard solution at a concentration of 100 mg/L.
- Solution B: Phenol solution dissolved in water at a concentration of 80% (w/w).
- Solution C: Concentrated Sulfuric acid (Analytical Grade).

In order to be able to quantify the total content of carbohydrates in a sample, a calibration curved is needed. Refer to Table 9 in appendix A to prepare the calibration curve. Once each tube had its corresponding concentration of glucose we proceeded to add the reagents in the following order. 50 μL of solution B was added, then 5 mL of solution C was added to each tube, directing the stream of the acid to the liquid rather than to the side of tube. Subsequently, the tubes were mixed with vortex and let stand for 10 min at 25°C. Finally each sample was read by spectrophotometry at 490 nm, it is important to mention that an unknown sample, be sure to dilute it with distilled water, such that the concentration is in the range of the calibration curve (10-50g/mL) and the sample volume is set to 2 mL.

3.8 Quantification of Ammonia

In order to run this method based on the protocol established by Koroleff [9] first is necessary to prepare the following stock solutions.

- Solution A : Solution of Phenol at a concentration of 100 g/L dissolved in ethanol 95% (v/v).
- Solution B : Solution of Sodium nitroferrocyanide at a concentration of 5 g/L.
- Solution C : Solution of Sodium hydroxide at a concentration of 10 g/L.
- Solution D : Oxidizing Solution made by mixing 100 mL of commercial sodium hypochlorite with 25 mL of solution C.
- Solution E: Stock solution of sulfate ammonia at a concentration of 27.72 mM. This solution is equivalent to a concentration of 1000 ppm of ammonia.

To quantify ammonia in the medium was necessary to construct a calibration curve prepared following the table 10 (Appendix A). It is important to mention that all glassware (screw cap test tubes were used) before use was scrubbed with neutral phosphates detergent and hot water, then rinse with 0.1 M HCl and vigorously agitate them. Finally the remaining of the acid were washed rinsing several times with de-ionized filtered water and were dried out in a convection oven at 75 °C. Once each tube has its corresponding concentration of ammonia (Table 11) is time to develop the reaction. First

we added to each tube, 40 μL of solution A, then 40 μL of solution B, following by the addition of 100 μL of solution D. Finally each tube was mixed with a vortex and let them sit in the darkness for 1.5 h, to let develop the reaction, then read the samples by spectrophotometry at 630 nm. It is important to highlight, that the samples must be mixed once half of the develop time has occurred. For an unknown sample, be sure to dilute it with distilled water, such that the concentration is in the range of the calibration curve (200-1000 μg/L) and the sample volume is set to 1 mL.

3.9 Method for solving the linear system of equations

A linear system of equations may have no answer. If it has answer may be a unique solution or a set of solution this will depend on the degrees of freedom of the system. Finally the system of linear equation proposed was solved using a Gaussian elimination which is one of several methods that can be used.

4 Results and Discussion

4.1 Experimental Fluxes

In order to calculate the fluxes of the model proposed, it is important to measure some experimental data as to fed the mathematical model with them. Therefore, biomass, substrate, nitrogen source and three products were measured. The six measured fluxes are presented in Table 7. It is important to mention that in order to guarantee that these values were measured under steady-state conditions, first we pumped at least 6.667 volumes of reactor. Second, the measurements from the sample of the "steady state" and the samples taken 24 h before were compared. The results of concentrations of ammonia, glucose and biomass did not show significant difference, which suggested that the culture achieved a steady state. In addition, in order to establish the concentration of ammonia in the medium, the theoretical yield of ammonia using the following stoichiometric equation, stating the empirical formation of biomass [28]:

$$\theta C_6H_{12}O_6 + \alpha NH_3 + \beta O_2 -> 2.36CH_{1.44}O_{0.5}N_{0.1} + \gamma CO_2 + \epsilon H_2O$$

Being θ, α, β, γ, and ϵ the stoichiometric coefficient of each compound. The ammonia coefficient obtained by a mass balance per element was, 0.236 mol. The theoretical yield of biomass per gram of NH_3 is defined as the relation between the stoichiometric coefficient of ammonia and biomass, $Y_{\frac{x}{NH_3}}$, as shown in the following equation:

$$Y_{X/NH3} = (\frac{2.36C_{mol}}{0.236mol_{NH3}})(\frac{22.84g_{cell}}{1C_{mol}})(\frac{1mol_{NH3}}{17.03g_{NH3}}) = 13.4\frac{g_{cell}}{g_{NH3}}$$

Meaning that the yeast biomass formed per gram of ammonia is 13.4 g, if and only if, the ammonia is the limiting substrate. Subsequent, we defined the minimum supply of carbon source in order to do not limit the ammonia as the relation between the yield of biomass on substrate, $Y_{\frac{X}{s}}$,and the yield of biomass on ammonia,$Y_{\frac{X}{NH_3}}$, as follows:

$$C/N = \frac{Y_{\frac{X}{NH_3}}}{Y_{\frac{X}{s}}} = 27.6$$

In this sense, relation of C/N with a coefficient higher than 27.6 the ammonia is being limited and relation lower than 27.6 the ammonia is not being limited. This is why the limited and non limited conditions were carried out having 1 and 0.5 g/L of ammonia and having 5 and 10 g/L of glucose, respectively.

It can be observed from Table 7 that the formation flux of astaxanthin under limited condition of ammonia is, significantly different from the formation flux under non limited condition, in other words,

the formation of astaxanthin flux is being promoted when the ammonia assimilation flux is limited. In this sense, what we defined as ammonia limitation, it can be expressed as a high carbon-nitrogen relation, C/N. The promotion of the accumulation of astaxanthin at low carbon levels has been studied and they have reported the highest concentrations of astaxanthin, carotenoids and biomass when a high C/N ratio was supplied to the culture [20], making sense with what we obtained. Furthermore, regarding the formation flux of carotenoids under non-limited ammonia assimilation, it appears to be a bit higher, suggesting that even though carotenoids were formed and instead of being used for astaxanthin production were deviated through the monocyclic carotenoid pathway as proposed in reference [11].

Table 7: Measured Fluxes under limited and non limited ammonia assimilation

Flux	**Non-Limited**	**Limited**	**Units**
Biomass q_x	0.036± 6 x10-04	0.0168± 2 x10-04	1/h
Glucose $q_{s/x}$	0.074± 9 x10-04	0.039± 2.7 x10-04	g/g-cell h
Ammonia $q_{n/x}$	0.004± 4.3 x10-05	0.002± 1.1 x10-05	g/g-cell h
Carbohydrates $q_{carbs/x}$	0.014± 1.7 x10-04	0.010± 7.4 x10-05	g/g-cell h
Carotenoids $q_{car/x}$	1382± 20	940.1± 6.5	μg/g-cell h
Astaxanthin $q_{ast/x}$	—-	86.4± 6 x10-01	μg/g-cell h

[a] Limited: 10 g/L Glucose, 0.5 g/L Ammonium sulfate; Non-Limited: 5 g/L Glucose, 1 g/L Ammonium sulfate

4.2 Metabolic Network and Mathematical model

Setting a mathematical model that estimates all of the 85 net rates established by the stoichiometric equations(shown in appendix B), with the six experimental fluxes that were measured (shown in Table 7) results in an infinite number of estimations. In this sense, a simplification analysis of the metabolic network was done in four phases in order to state a mathematical model with a finite number of solutions. First, all the metabolic reactions that were linear were summed up and stated as a global net flux. in section 4.2.1 is explained with detail which criteria was established in each metabolic block in order to be simplified. Second the compartmentalization within the cell was neglected, taking out of the model different mitochondrial and extracellular chemical species. Third, the simplified stoichiometry and differential molar balances were stated, as shown in section 4.2.1, and 4.2.2, respectively, in order to established the system of equations. Finally, the system of equations was proposed with 34 intracellular fluxes (columns) and 31 molar balances (rows). After solving the system by Gaussian eliminations it was elucidated two thing. On one hand, the intracellular fluxes leaved out of the system are the following: r_6, r_{22}, r_{24}, r_{32}, r_{33}, r_{34}, r_{36}, r_{37}, r_{39}, r_{43}, and r_{44} which correspond to the number of stoichiometric reaction stated in section 4.2.1. On the other, the measured fluxes used to feed the model were $q_{\frac{s}{x}}$(Glucose assimilation flux), $q_{\frac{NH_3}{x}}$(Ammonia assimilation flux), and $q_{\frac{ast}{x}}$ (Astaxanthin formation flux) r_1, r_{40}, and r_{30}, respectively.

4.2.1 Stoichiometry of the Simplified Metabolic Network

Glycolysis

From the 11 stoichiometric reactions stated in the complete pathway (See Appendix B; Glycolysis) the equations 3-7 and 8-11 were summed up. The criteria to keep this metabolites is because they are branch point for the other metabolic pathways. Leaving the next six stoichiometric equations

1. $\frac{1}{2}$ Glu + ATP_c $\longrightarrow$ $\frac{1}{2}$ G6P + ADP
2. $\frac{1}{2}$ G6P $\longrightarrow$ $\frac{1}{2}$ F6P
3. $\frac{1}{2}$ F6P + ATP_c $\longrightarrow$ G3P + ADP
4. G3P +NAD^+ + ADP $\longrightarrow$ 3PG + NADH + ATP_c
5. 3PG + ADP $\longrightarrow$ Pyr + ATP
6. Pyr $\longrightarrow$ Pyr_m

Tri-Carboxylic Acid Cycle

The only two equations that were simplified were 18-19 (Appendix B; TCA cycle). Leaving as result the following 10 stoichiometric equations.

7. Pyr_m + NAD^+ + CoA $\longrightarrow$ $AcCoA_m$ + CO_{2c} + NADH
8. $AcCoA_m$ + OXA $\longrightarrow$ CIT_m + CoA
9. CIT_m $\longrightarrow$ IsoCIT
10. IsoCIT + NAD^+ $\longrightarrow$ AKG + CO_{2c} +NADH
11. IsoCIT $\longrightarrow$ GOX + Succ
12. GOX + $AcCoA_m$ $\longrightarrow$ MAL + CoA
13. AKG + NAD^+ + ADP $\longrightarrow$ SUCC + NADH + ATP_m + CO_{2c}
14. SUCC + FAD^+ $\longrightarrow$ FUM + FADH
15. FUM $\longrightarrow$ MAL_m
16. MAL_m + NAD^+ $\longrightarrow$ OXA + NADH

Pentose Phosphate Pathway

In this metabolic block instead of being in carbon balance, as shown in Appendix B, is stated in molar balance in order to maintain consistency along the network that is being mol balanced. The stoichiometric equations summed up were reactions 23-27(Appendix B; Pentose Phosphate Pathway), resulting in the five stoichiometric equations as follows:

17. $\frac{1}{2}$ G6P + $\frac{1}{2}$ ATP_c + $NADP^+$ $\longrightarrow$ $\frac{1}{2}$ R5P + $\frac{1}{2}$ ADP + NADPH + $\frac{1}{2}$ CO_2
18. $\frac{1}{2}$ R5P $\longrightarrow$ $\frac{1}{2}$ XYL5P
19. $\frac{1}{2}$ R5P + $\frac{1}{2}$ XYL5P $\longrightarrow$ $\frac{1}{2}$ S7P + $\frac{1}{2}$ G3P
20. $\frac{1}{2}$ S7P + $\frac{1}{2}$ G3P $\longrightarrow$ $\frac{1}{2}$ E4P + $\frac{1}{2}$ F6P
21. $\frac{1}{2}$ XYL5P + $\frac{1}{2}$ E4P $\longrightarrow$ $\frac{1}{2}$ F6P + $\frac{1}{2}$ G3P

Lipid Synthesis

Regarding this metabolic block only the transport of citrate, stoichiometric equation 22, was excluded from the model.

22. CIT_m $\longrightarrow$ CIT
23. CIT + ATP_c + CoA $\longrightarrow$ AcCoA + OXA + ADP
24. 8 AcCoA + 7 ATP_c + 14 NADPH $\longrightarrow$ α Biomass + 14 $NADP^+$ + 7 ADP + 8 CoA

Mevalonate Pathway

The mevalonate synthesis block was summed up from the stoichiometric equation 35-42 (Appendix B; Mevalonate Pathway), stated as the following global stoichiometric equation. this could be done because there were not branch points connecting with other pathway.

25. 3 AcCoA + 2NADPH + 3 ATP_c $\longrightarrow$ IPP + 2 $NADP^+$ + 3 ADP + CO_2 + 3 CoA

Carotenoid Synthesis

The carotenoid synthesis pathway was summed up as follow: stoichiometric equations from 47 to 49, 50 to 52, 53 to 54, 58 to 60, and 55-57 plus 61-63, resulting in the stoichiometric equations 26, 27, 28, 29, and 30, respectively. It is important to mention that the synthesis of ergosterol (EGS) was not considered in this metabolic network, however, this may represent an important branch where farnesyl-PP (FPP) is diverged to the synthesis of EGS instead of being used for the carotenoid synthesis. For making this model more sensitive, EGS would be an important metabolite to monitored in order to confirmed if FPP is being used to synthesized EGS instead of β-carotene and its derivatives, due to the lack of NADPH bio-availability, which is required as a proton donor.

26. 4 IPP $\longrightarrow$ GGPP + 3PP

27. 2 GGPP + 4 $NADP^+$ $\longrightarrow$ LYC + 4 NADPH

28. LYC $\longrightarrow$ β-Car

29. LYC + 2 O_2 $\longrightarrow$ HDCO

30. 2 β-Car + 9 NADPH + 12 O_2 $\longrightarrow$ 2 Ast + 9 $NADP^+$

Oxidative Phosphorylation

For the simplification of the oxidative phosphorylation a global stoichiometric equation was obtained from the sum of the equations 43-45(Appendix B; Oxidative Phosphorylation), resulting in the following equation. It is important to remind that compartmentalization within the cell was neglected, thus leaving stoichiometric equation 32 out of the system.

31. NADH + FADH + ADP + Pi + 5 O_2 $\longrightarrow$ 5 ATP_m

32. ATP_m $\longrightarrow$ ATP_c

Transhydrogenase Cycle

We intended to conserved this metabolic block , however, the mathematical analysis showed that with the available measured fluxes we have to only include equation 35.

33. Pyr + ATP_c + CO_{2c} $\longrightarrow$ OXA + ADP

34. OXA + NADH $\longrightarrow$ MAL + NAD^+

35. MAL + $NADP^+$ $\longrightarrow$ Pyr + NADPH + CO_{2c}

36. NAD^+ + ATP_c $\longrightarrow$ $NADP^+$ + ADP

37. MAL $\longrightarrow$ MAL_m

Protein Synthesis

For the simplification of the Protein synthesis block a global equation is established as follows, summing up equations 70-78 (Appendix B; Protein Synthesis) resulting as the following equation.

38. 2 Pyr + E4P + AcCoA + OXA + AKG + 3PG + R5P + GLUT + GLA $\longrightarrow$ β Prot

Ammonium Assimilation

The only reaction disregarded in the model is the stoichiometric equation 39.

39. NH_3 $\longrightarrow$ NH_{3c}

40. NH_{3c} + AKG + NADPH $\longrightarrow$ GLUT + $NADP^+$

41. NH_{3c} + GLUT + ATP_c $\longrightarrow$ GLA + ADP

Structural Carbohydrates Synthesis

This block remained intact.

42. NH_{3c} + GLA + AcCoA + F6P + 2 ATP_c $\longrightarrow$ α Carbs + 2 ADP

Synthesis of Nucleic Acids

The synthesis of nucleic acids was not included in the mathematical due to the mathematical analysis done it could not be considered in this model. However, as stated before to add sensitivity to this model either, include it as a calculated or measured flux.

43. 8 R5P + 4 OXA + 4 3PG + 64 ATP_c + 36 NH_{3c} + 11 NADPH + 12 NAD^+ $\longrightarrow$

α_2 Biomass + 64 ADP + 11 $NADP^+$ + 12 NADH

Gas Transfer medium-cell

Only the formation of CO_2 was included in the model, which correspond to the stoichiometric equation 45.

44. $O_2 \longrightarrow O_{2c}$

45. $CO_2 \longrightarrow CO_{2ec}$

4.2.2 Differential Molar Balance per metabolite

First, it is important to state that all of the following balances are under steady-state condition, meaning that the change of concentration of any intracellular metabolite with respect of time does not change, $\frac{d[met_i]}{dt} = 0$, being met_i any of the following metabolites and reaction flux, r_i, and it subindex correspond to the ones illustrated in Figure 9. Second, all the metabolites considered in this balance are those besides the extracellular and mitochondrial metabolites, and for the electron carriers only its reduced state was taken into account. It is important to mention that the balances of ammonia, NH_3, astaxanthin, Ast, and glucose, Glu, are measured fluxes. Resulting in the following set of balances:

1. $\frac{d[Glu]}{dt} = 0 = -0.5\ r_1$
2. $\frac{d[G6P]}{dt} = 0 = 0.5\ r_1 - 0.5\ r_2 - 0.5\ r_{17}$
3. $\frac{d[F6P]}{dt} = 0 = 0.5\ r_2 - 0.5\ r_3 + 0.5\ r_{20} + 0.5\ r_{21} - r_{42}$
4. $\frac{d[G3P]}{dt} = 0 = r_3 - r_4 + 0.5\ r_{19} - 0.5\ r_{20} + 0.5\ r_{21}$
5. $\frac{d[3PG]}{dt} = 0 = r_4 - r_5 - 3\ r_{38}$
6. $\frac{d[Pyr]}{dt} = 0 = r_5 - r_7 - r_{33} + r_{35} - 2\ r_{38}$
7. $\frac{d[AcCoA]}{dt} = 0 = r_7 - r_8 - r_{12} + r_{23} - 3\ r_{25} - r_{38} - r_{42}$
8. $\frac{d[CO_2]}{dt} = 0 = r_7 + r_{10} + r_{13} + 0.5\ r_{17} + r_{25} - r_{33} + r_{35} - r_{45}$
9. $\frac{d[OXA]}{dt} = 0 = -r_8 + r_{16} + r_{23} + r_{33} - r_{34} - r_{38}$
10. $\frac{d[CIT]}{dt} = 0 = r_8 - r_9 - r_{23}$
11. $\frac{d[IsoCIT]}{dt} = 0 = r_9 - r_{10} - r_{11}$
12. $\frac{d[AKG]}{dt} = 0 = r_{10} - r_{13} - r_{38} - r_{40}$
13. $\frac{d[GOX]}{dt} = 0 = r_{11} - r_{12}$
14. $\frac{d[SUCC]}{dt} = 0 = r_{11} + r_{13} - r_{14}$
15. $\frac{d[MAL]}{dt} = 0 = r_{12} + r_{15} - r_{16} + r_{34} - r_{35}$
16. $\frac{d[FUM]}{dt} = 0 = r_{14} - r_{15}$
17. $\frac{d[R5P]}{dt} = 0 = 0.5\ r_{17} - 0.5\ r_{18} - 0.5\ r_{19} - r_{38}$
18. $\frac{d[XYL5P]}{dt} = 0 = 0.5\ r_{18} - 0.5\ r_{19} - 0.5\ r_{21}$

19. $\frac{d[S7P]}{dt} = 0 = 0.5\ r_{19} - 0.5\ r_{20}$

20. $\frac{d[E4P]}{dt} = 0 = 0.5\ r_{20} - 0.5\ r_{21} - r_{38}$

21. $\frac{d[IPP]}{dt} = 0 = r_{25} - 4\ r_{26}$

22. $\frac{d[GGPP]}{dt} = 0 = r_{26} - 2\ r_{27}$

23. $\frac{d[LYC]}{dt} = 0 = r_{27} - r_{28} - r_{29}$

24. $\frac{d[\beta-Car]}{dt} = 0 = r_{28} - 2\ r_{30}$

25. $\frac{d[HDCO]}{dt} = 0 = r_{29}$

26. $\frac{d[Ast]}{dt} = 0 = 2\ r_{30}$

27. $\frac{d[O_2]}{dt} = 0 = -\ 2\ r_{29} - 12\ r_{30} - 5\ r_{31} + r_{44}$

28. $\frac{d[GLUT]}{dt} = 0 = r_{40} - r_{41} - r_{38}$

29. $\frac{d[GLA]}{dt} = 0 = r_{41} - r_{42} - r_{38}$

30. $\frac{d[NH_3]}{dt} = 0 = r_{39} - r_{40} - r_{41} - r_{42}$

31. $\frac{d[Prot]}{dt} = 0 = r_{38}$

32. $\frac{d[Carbs]}{dt} = 0 = r_{42}$

33. $\frac{d[ATP]}{dt} = 0 = -\ r_1 - r_3 + r_4 + r_5 + r_{13} - 0.5\ r_{17} - r_{23} - r_{25} + 5\ r_{31} - r_{33} - r_{36} - r_{41} - 2\ r_{42}$

34. $\frac{d[NADH]}{dt} = 0 = r_4 + r_7 + r_{10} + r_{13} + r_{16} - r_{31} - r_{34}$

35. $\frac{d[NADPH]}{dt} = 0 = r_{17} - 2\ r_{25} + 4\ r_{27} - 9\ r_{30} + r_{35} - r_{40}$

36. $\frac{d[FADH]}{dt} = 0 = r_{14} - r_{31}$

4.2.3 Mathematical Model: A lineary independent and homogeneous system

After simplifying and elucidating which reactions should be taken account into the model, the matrix shown in Figure 7 was constructed with the system of equations stated in section 4.2.2 leaving out of the system the balances of protein, carbohydrates and HDCO (hydroxy-keto-torulene). This matrix was fed into Mathematica Wolfram in order to obtain the rank of the matrix to find out that the system has 31 linearly independent equations (metabolite mol balances) and 34 unknown variables (net fluxes). The metabolite balances were set as rows and the net fluxes as columns.

In order to defined which of the measured fluxes were going to be used, first, the row reduced form of the matrix in Fig. 7 was calculated giving as result the matrix illustrated in Figure 8. Identifying

that the system was solved in terms of the last three columns being r_{40}, r_{30}, and r_1 which correspond to the measurements of ammonia, astaxanthin, and glucose fluxes, respectively. This can be observed in the matrix illustrated in Figure 8, where the diagonal depict the linearly independent equations in terms of the last 3 columns of coefficients.

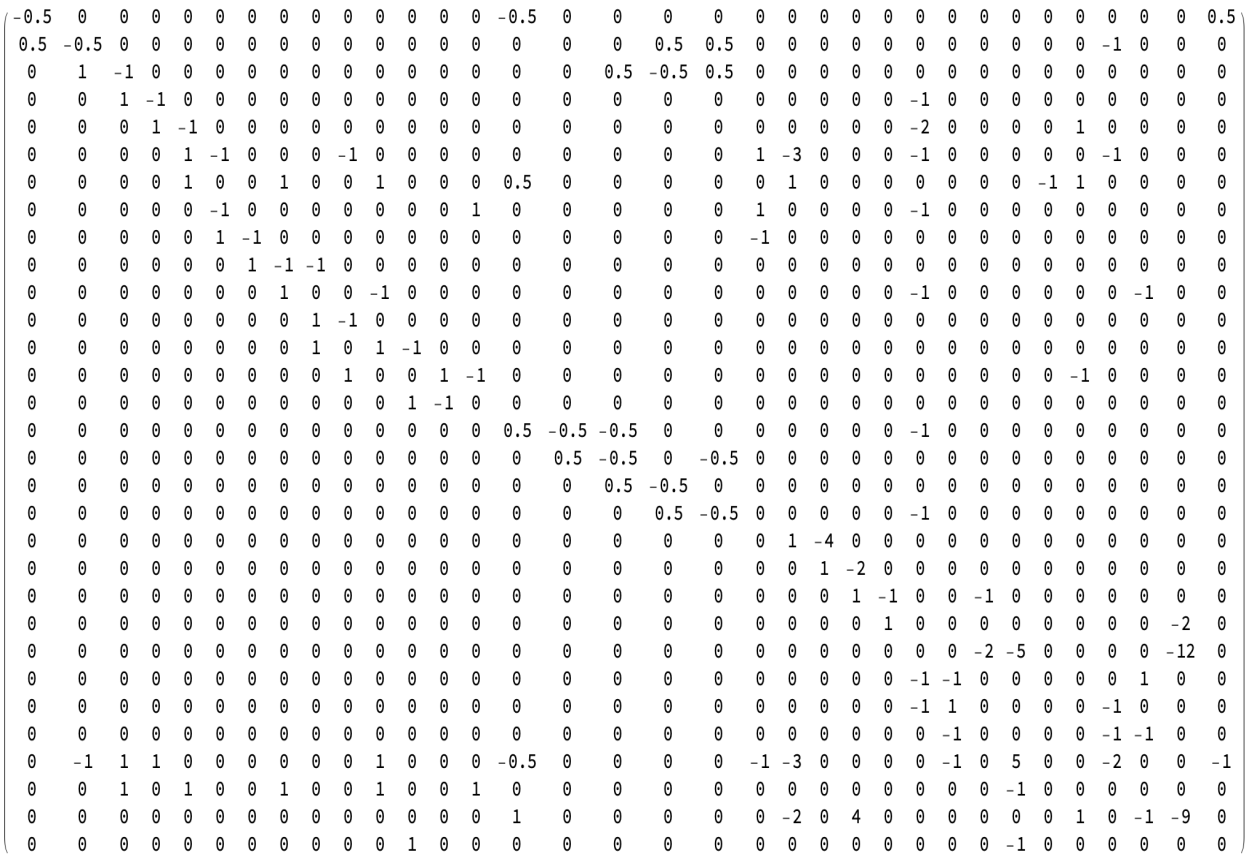

Figure 7: A linearly independent and homogeneous system of equations.

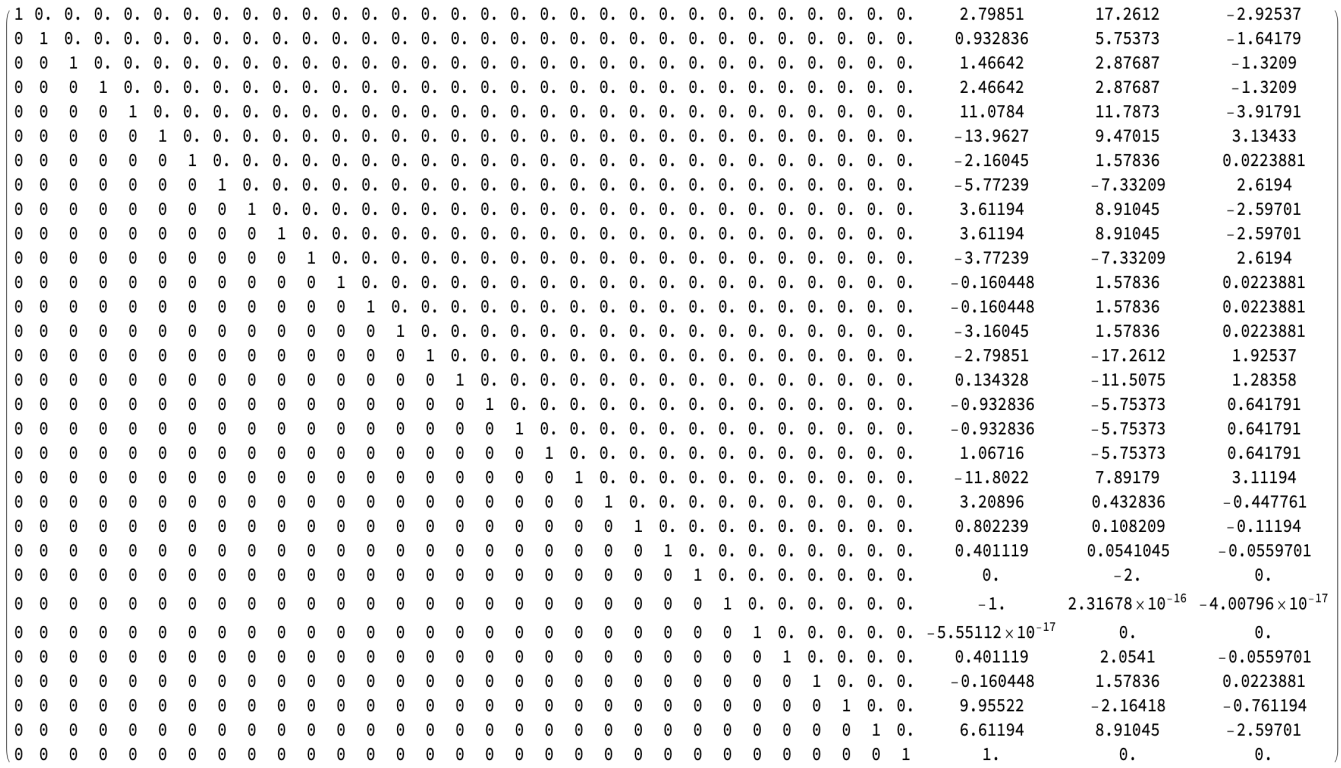

Figure 8: Row reduced form of Matrix in Figure 7.

4.3 Estimated Fluxes and the Integrated Metabolic Network of *X. dendrorhous*

In this section the constructed Metabolic network with the calculated fluxes in both steady-state conditions (non-limited and limited ammonia assimilation) is presented. It is important to mention that because balances were made in mol-basis the experimental fluxes had to be converted into proper units such as $\frac{mmol}{g-cellh}$. In order to do it, each flux was divided by its molecular weight and molar coefficient. The values obtained are shown in Table 8. Once they were fed into the model the intracellular fluxes under both conditions were estimated and used to build the metabolic network, which is illustrated in Figure 9. Here, it can be seen the distribution of the calculated fluxes obtained for solving the proposed mathematical model under limited and non-limited concentration of nitrogen.

Table 8: Measured Fluxes in units of $\frac{mmol}{g-cellh}$

Flux	**Limited**	**Non-Limited**
Glucose $q_{s/x}$	0.4363	0.8215
Ammonia $q_{n/x}$	0.1174	0.2349
Astaxanthin $q_{ast/x}$	7.2 E-05	—-

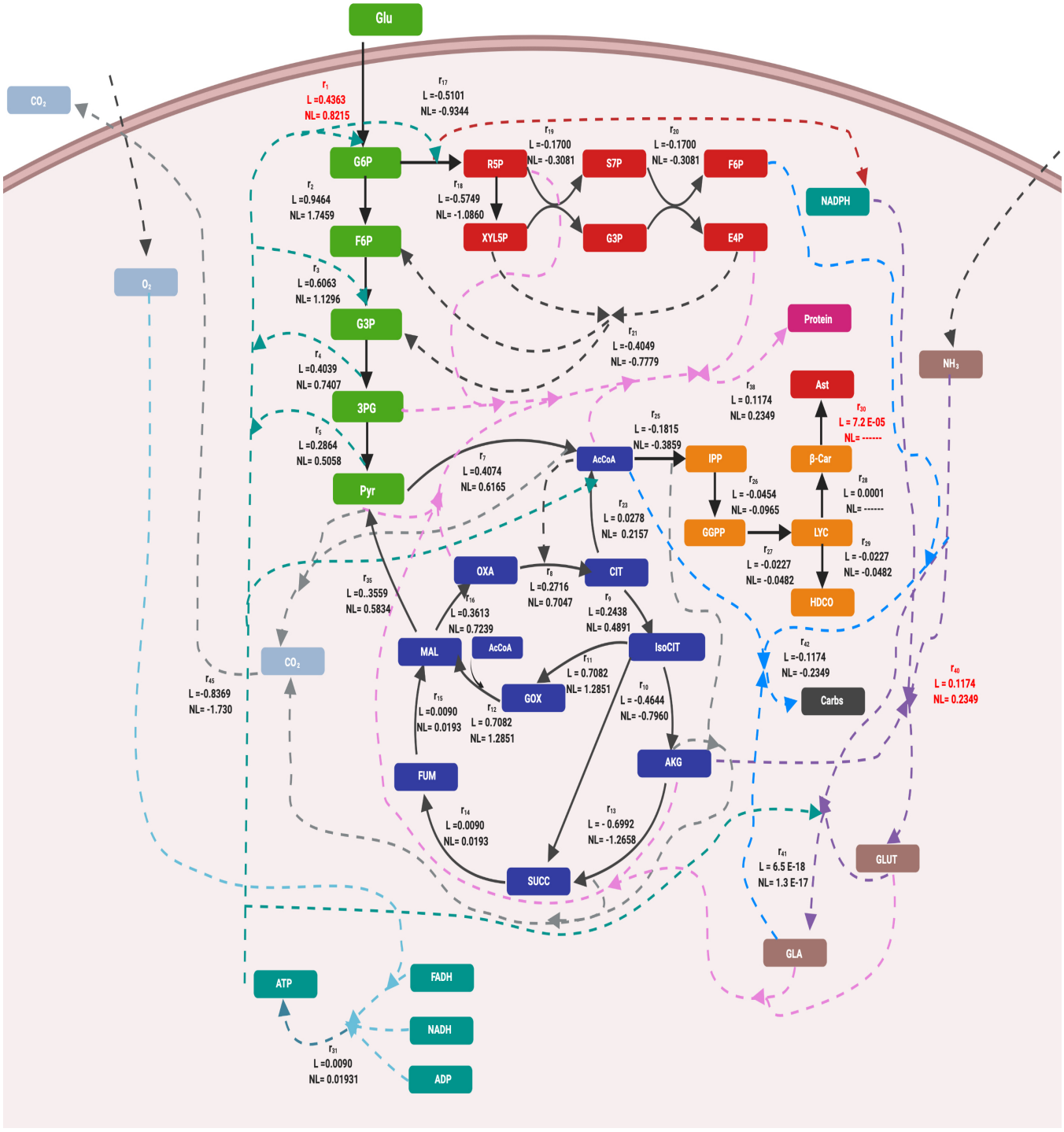

Figure 9: The fluxes in red, r_{40}, r_{30}, and r_1 correspond to molar experimental fluxes obtained, $q_{n/x}$, $q_{ast/x}$, and $q_{s/x}$, respectively. Molar fluxes ($\frac{mmol}{g-cellh}$) of different metabolic pathways involved in astaxanthin synthesis. L, limited, NL, non-limited ammonia assimilation flux, respectively. Green, Glycolysis; Blue TCA/Krebs cycle; Red, Pentose Phosphate Pathway (PPP); Orange, Carotenoid Synthesis; Pink, Protein Synthesis; Light Blue arrows, Structural Carbohydrates Synthesis; Purple Arrows Ammonia assimilation GOGAT and GS; Aqua, Oxidative Phosphorylation and sytnhesis of NADPH via PPP.

The net fluxes in the metabolic network of Figure 9 that were identified as indicators of whether the metabolic block was active or not were then chosen and illustrated in Figure 10. It is important to mention that a negative value of a calculated flux will mean that reaction related to this flux is not being favorable in the formation of the metabolite involved.

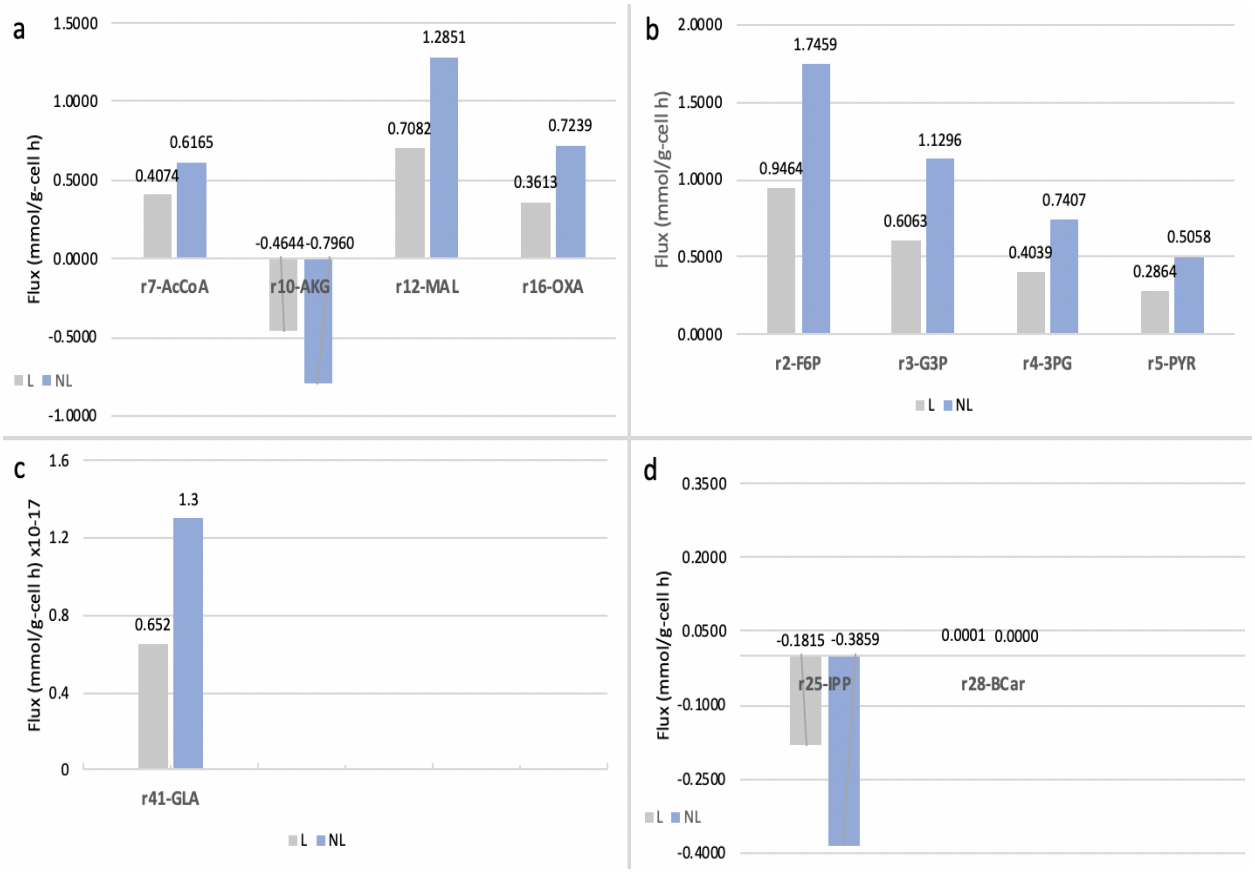

Figure 10: Calculated intracellular fluxes under limited (L) and Non-limited (NL) ammonia assimilation. The metabolite next to each flux represent that is being formed.(a) TCA/Krebs cycle, (b) Glycolysis, (c) Ammonia assimilation, (d) Carotenoid synthesis.

The fluxes of the TCA cycle illustrated in Figure 10a are r_7, r_{10}, r_{12}, and r_{16}, which are related to the formation flux of AcCoA from PYR, IsoCit to AKG, GOX to MAL, and MAL to OXA, respectively. This fluxes were selected in order to evaluate the attenuation of Krebs cycle and according to the values obtained the formation of α-ketoglutarate (formed by r_{10}) is not being promoted, hence the Krebs cycle is presumably active via glyoxylate (consumed by r_{12}) in both conditions, limited and non-limited. Even though, the cycle may be attenuated in both conditions, limited and non-limited, the reasons why is being diminished may be different. Under non-limited conditions, the glucose is being the limiting substrate, in this sense, it has been reported that under limiting conditions of glucose the glyoxylate cycle is activated in *S. cerevisiae*, which supports what we have proposed [16]. Under limited condition of ammonia assimilation, the isocitrate dehydrogenase, IDCH, is down-regulated,

explaining why the flux, r_{10} is negative and the glyoxylate cycle is activated (r_{12}) as a response of the glucose still being assimilated, as it has been reported in oleaginous microorganism [10].

As it can be observed from Figure10b the formation fluxes of F6P, G3P, 3PG and PYR, corresponding to r_2, r_3, r_4, and r_5 , respectively, are positive denoting that in both conditions of ammonia assimilation, the assimilation of glucose is still active via glycolysis as suggested by the model. In the case of the flux of assimilation of NH_3, presented as r_{41} in Figure10c, it is identified that the flux under non-limited condition is twice as compared to the flux under limited condition of ammonia. Therefore, it can be corroborated that this ammonia assimilation flux via glutamine (r_{41}) indeed is being limited in comparison to the non limited condition. Finally, regarding the formation fluxes of carotenoids, we have chosen the formation of IPP and β-carotene depicted in Figure10d as r_{25} and r_{28}, respectively, as indicators. Regardless of the negatives values estimated for r_{25}, under limited condition the flux is twice the flux obtained under non limited, suggesting that the NH_3 limitation is causing a metabolic change that promotes the formation of carotenoids, as is depicted in the β-carotene formation flux, r_{28}(see Fig. 10d), where there was not formation of this carotenoid under non-limited condition, while, under limited condition of nitrogen formation of this carotenoid was promoted.

The key precursor for lipid accumulation in oleaginous microorganism is AcCoA, however, this metabolite will be only available by limitation of nitrogen but in presence of glucose. The accumulation of AcCoA occurs thanks to Isocitrate dehydrogenase, ICDH, which is an AMP dependant enzyme. Unfortunately, when the microorganism is at critical level of nitrogen, an ammonia donor system is activated, the AMP deaminase, which takes the ammonium from AMP transforming it into IMP. Due to the depletion of AMP, IDCH is deactivated, causing the rapid accumulation of isocitrate, and as isocitrate is accumulated and no longer metabolized, citrate as well starts to build-up via Aconitase. Subsequently, citrate is translocated from the mitochondria to the cytosol via Malate/Citrate translocase system. Finally, once in the cytosol, citrate is transformed into AcCoA and oxaloacetate by the ATP citrate Lyase, ACL [10].

In the case of *X. dendrorhous*, we have proposed that these same pool of reactions converging in AcCoA byosynthesis is used by this yeast for synthesis of isopentyl pyrophosphate, IPP, via mevalonate, which is the basic formation unit for any other carotenoid. the flux r_{23} (formation of AcCoA from CIT), shown in Figure 11, it is proposed to be associated to the activity of ACL. Under limited versus non-limited ammonia assimilation this accumulation flux appears to be 10 time higher with no limitation as it can be observed in Figure 11. Nonetheless, as it represents net formation this may suggests that AcCoA is being used as a biosynthesis unit for lipids, carotenoids or both under the limiting condition. Chavez-Cabrera and his collaborators suggest that, ACL may be the provider of AcCoA used for carotenoid synthesis, however they could not conclude if its activity was enhanced due to the limitation of ammonia [6]. Either if limitation of ammonia assimilation enhance or not the activity of ACL, the estimated fluxes obtained from the mathematical model may imply that this enzyme is

stimulated within the conditions established in each steady state condition. Moreover, a recent study correlated higher biomass, carotenoid and astaxanthin content with very high relation of C/N (76:1). However, the specific content of cellular carotenoid and astaxanthin decreased, meaning the that the overall concentration of astaxanthin and carotenoid increased due to the biomass increment [20]. It is noteworthy to mention that in this study authors supplemented the medium with a high concentration of yeast extract, a complex source of both carbon and nitrogen. This suggests that it is possible that the yeast was not under limiting conditions of nitrogen, thus not impacting the cellular growth and leading to astaxanthin and carotenoid accumulation due to the increment on biomass.

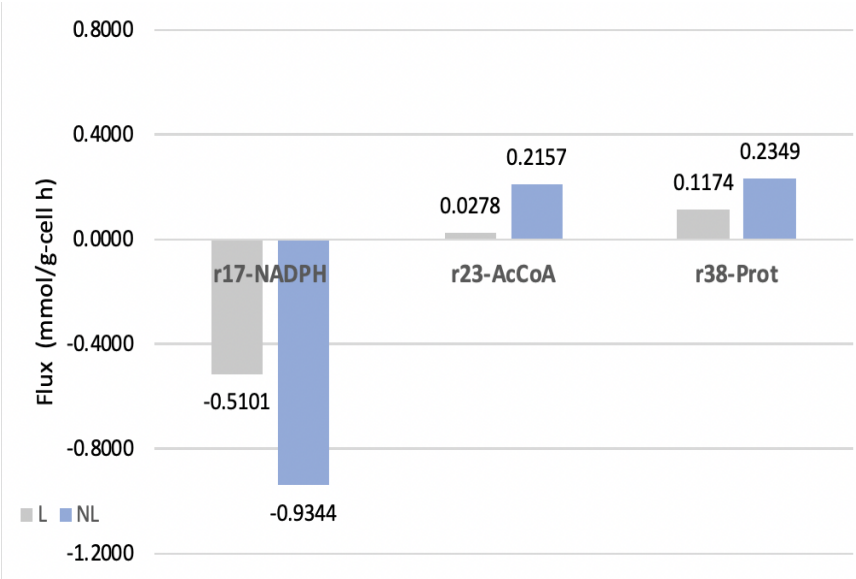

Figure 11: Calculated intracellular fluxes under limited (L) and Non-limited (NL) ammonia assimilation. This three fluxes are being proposed as some of the important key points for the synthesis of astaxanthin

Another key point proposed in the biosynthesis of carotenoids is the bio-availability of NADPH as an electron donor in the cyclation and desaturation of β-carotene, electron carrier neccesary to transform the latter into astaxanthin. It has been reported that when a yeast grows in presence of ammonia as the sole nitrogen source, the bio-availability of this source has a significant effect on the amount of carbon skeletons, ATP and NADPH that are used as precursor for protein synthesis [5]. From the estimated fluxes r_{17}, and r_{38}, related to NADPH and protein synthesis, respectively, it can be identified that there was a change between the fluxes of each steady state condition (Figure 11). In this figure, the flux of protein formation, r_{38}, is being promoted, but there is a deficit of NADPH formation flux, r_{17}, therefore, it may be suggested that growth on ammonia as a sole source of nitrogen deviate the flux of carbohydrates and NADPH towards protein synthesis.

Finally, with the estimated fluxes, r_7, r_{10} r_{12}, and r_{16}, which correspond to the formation fluxes of AcCoA from PYR, AKG from IsoCIT, MAL from GOX, and MAL to OXA, respectively. An observable change of the TCA/Krebs cycle is elucidated showing as result, that the formation of citrate is being promoted. However, under non limited condition of ammonia assimilation there is no formation of either carotenoid and astaxanthin. In contrast, under limited condition, the carotenoid formation flux seems to open just a little, leading to formation of astaxanthin. This strongly suggest that the control mechanism of astaxanthin biosynthesis is correlated with the assimilation flux of ammonia. Thus by limiting this assimilation flux may be a strategy to promote the synthesis of astaxanthin. However, in order to conclude it with determination further experiments are needed. Such as, another limiting ammonia assimilation condition one that let us elucidate a direct impact on the formation of biomass. To conclude, what this model permitted, as a first approximation, was to identify that AcCoA is involved as an essential precursor for carotenoid and astaxanthin synthesis, in addition the reducing power supply of NADPH instead of being estimated may be measured in order to corroborate the different deviations it has under steady state condition.

5 Conclusions and Perspective

Different approaches to enhance astaxanthin production in *Xanthophyllomyces dendrorhous* are continuously done. Nonetheless, how astaxanthin is produced, which key metabolites are necessary, which are the regulatory mechanisms of the pathway, and which enzymes govern the key metabolic processes, are just some of the remaining questions regarding this microorganism. A better and integrated understanding of the metabolism of *X. dendrorhous* may lead to answer some of these questions.

In this work, the metabolic flux analysis of the metabolism of *X. dendrorhous* was performed under limited and non-limited ammonia assimilation conditions at steady state conditions. As expected, when the yeast was grown under limited conditions of ammonia, the formation flux of astaxanthin was increased suggesting that the limitation of ammonia assimilation makes the cell use as an alternative source of nitrogen such as, AMP via AMP deaminase, in consequence the levels of AMP decrease resulting in an arrest of the Krebs cycle at the level of AMP-dependant isocitrate dehydrogenase (ICDH), as isocitrate is accumulated citrate is also being accumulated. Finally this accumulation of citrate results in a promotion of the accumulation of AcCoA, which is the basic formation unit for lipid and carotenoid synthesis.

The Metabolic Flux Analysis has proven to be a valuable tool as an approach to study the metabolism of *X. dendrorhous*. First there are no ambiguities on how to defined a limitation of a substrate, this turnout to be of upmost important for elucidating perturbations on different blocks of the metabolism. Second, for this analysis to be highly sensitive more experimental fluxes must be determined, in order to make a more complex system and estimate other important fluxes, however, it allowed to confirm that the formation of astaxanthin is promoted under limiting conditions of ammonia assimilation. In addition, studying the biochemistry of the system one may be able to construct high output models with just the necessary measurement for obtaining important information of the metabolic network.

Regarding the application of the MFA for studying the the intracellular fluxes of important metabolites such as AcCoA and NADPH and their role in carotenoid synthesis another limitation condition must be obtained. Nonetheless, it is important to mention that due to the solid prove that limiting ammonia assimilation promote the formation of astaxanthin, further works may be done in order to explore in more detail how the limitation controls the metabolism, or even different genetic engineering approaches may be addressed elucidate the physiological state. With the final objective of understand the astaxanthin synthesis as an integrated pathway of a whole metabolism system and eventually identify the key control nodes, as result, be able to propose synthetic pathways affecting the minimum possible the necessities of the system.

6 Appendixes

6.1 Appendix A

Table 9: Volumes that each test tube has to have in order construct the calibration curve.

Concentration (mg/mL)	**Glucose Solution (mg/mL)**	**Distilled Water**
0	0μL	1000μL
0.1	100μL	900μL
0.2	200μL	800μL
0.3	300μL	700μL
0.4	400μL	600μL
0.5	500μL	500μL
0.6	600μL	400μL
0.7	700μL	300μL
0.8	800μL	200μL
0.9	900μL	100μL
1.0	1000μL	0μL

Table 10: Volumes that each test tube has to have in order construct the calibration curve.

[Glucose Equivalents](μg/mL)	**Glucose Solution (100 μg/mL)**	**Distilled Water**
50	1000μL	1000μL
40	800μL	1400μL
30	600μL	1800μL
20	400μL	1200μL
10	200μL	1600μL
0	0μL	2000μL

Table 11: Volumes that each test tube has to have in order construct the calibration curve.

Concentration NH_4 (μg/L)	**Ammonia Solution (1000 μg/L)**	**Distilled Water**
1000	1000μL	0μL
800	800μL	200μL
600	600μL	400μL
400	400μL	600μL
200	200μL	800μL
0	0μL	1000μL

Table 12: Table of Nomenclature.

Compound	**Abbreviation**
Glucose	Glu
Glucose 6 Phosphate	G6P
Fructose 6 Phosphate	F6P
Glyceraldehyde 3 Phosphate	G3P
3, Phosphoglycerate	3PG
Pyruvate	Pyr
Mitochondrial Pyruvate	Pyr_m
oxaloacetate	OXA
Malate	MAL
Mitochondrial Malate	MAL_m
Ribose 5 Phosphate	R5P
Xylulose 5 Phosphate	XYL5P
Sedoheptulose 7 Phosphate	S7P
Erythrose 4 Phosphate	E4P
Acetyl Co-enzyme A	AcCoA
Mitochondrial Acetyl Co-enzyme A	AcCoA_m
Citrate	CIT
Mitochondrial Citrate	CIT_m
Isocitrate	IsoCIT
Alpha-ketoglutarate	AKG
Succinate	SUCC
Fumarate	FUM
Flavin Adenine Dinucleotide Oxidized	FAD^+
Flavin Adenine Dinucleotide Reduced	FADH
Nicotine Adenine Dinucleotide Oxidized	NAD^+
Nicotine Adenine Dinucleotide Reduced	NADH
Nicotine Adenine Dinucleotide Phosphate Oxidized	NADP^+
Nicotine Adenine Dinucleotide Phosphate Reduced	NADPH
Adenosine Triphosphate	ATP
Adenosine Diphosphate	ADP
Isopentyl Pyrophosphate	IPP
Geranyl Pyrophosphate	GPP
Farnesyl Pyrophosphate	FPP
Ergosterol	EGS
Geranyl Geranyl Pyrophosphate	GGPP

Continuation of Table 12	
Compound	**Abbreviation**
Phytoene	Phy
Neurosporene	NSR
Lycopene	LYC
Didehydrolycopene	DHLYC
Torulene	TOL
3-Hydroxy-4-ketotorulene	HDCO
γ-Carotene	γ-Car
β-carotene	β-Car
Echinone	ECNO
Phoenicoxanthin	PCX
Criptoxanthin	CRX
Adoxanthin	ADX
Astaxanthin	Ast
Cytosolic Carbon Dioxide	CO_{2c}
Cytosolic Oxygen	O_{2c}
Cytosolic Ammonia	NH_{3c}
Carbon Dioxide in medium	CO_2
Oxygen in medium	O_2
Ammonia in medium	NH_3
L-Glutamate	GLUT
L- Glutamine	GLA
Protein	Prot
Carbohydrates	Carbs
Biomass	Biomass
Pyrophosphate	PP

6.2 Appendix B

Stoichiometry of the metabolic Network

Glycolysis

1. Glu + ATP_c $\longrightarrow$ G6P + ADP
2. G6P $\longrightarrow$ F6P
3. F6P + ATP_c $\longrightarrow$ F1,6P + ADP
4. F1,6P $\longrightarrow$ $\frac{1}{2}$ DHAP + $\frac{1}{2}$ G3P
5. DHAP $\longrightarrow$ G3P
6. G3P +NAD^+ $\longrightarrow$ G1,3P + NADH
7. G1,3P +ADP $\longrightarrow$ 3PG + ATP_c
8. 3PG $\longrightarrow$ 2PG
9. 2PG $\longrightarrow$ PEP
10. PEP + ADP $\longrightarrow$ Pyr + ATP_c
11. Pyr $\longrightarrow$ Pyr_c

Tri-Carboxylic Acid Cycle

12. Pyr_c + NAD^+ + CoA $\longrightarrow$ $AcCoA_m$ + CO_{2c} + NADH
13. $AcCoA_m$ + OXA $\longrightarrow$ CIT_m + CoA
14. CIT_m $\longrightarrow$ IsoCIT
15. IsoCIT + NAD^+ $\longrightarrow$ AKG + CO_{2c} +NADH
16. IsoCIT $\longrightarrow$ GOX + Succ
17. GOX + $AcCoA_m$ $\longrightarrow$ MAL + CoA
18. AKG + NAD^+ + CoA $\longrightarrow$ SCoA + NADH + CO_{2c}
19. SCoA + ADP $\longrightarrow$ SUCC + ATP_m + CoA
20. SUCC + FAD^+ $\longrightarrow$ FUM + FADH
21. FUM $\longrightarrow$ MAL_m

22. MAL_m + NAD^+ $\longrightarrow$ OXA + NADH

Penthose Phosphate Pathway

23. G6P + ATP_c $\longrightarrow$ GL6P + ADP
24. GL6P $\longrightarrow$ GLT
25. GLT + ATP_c $\longrightarrow$ GLT6P + ADP
26. GLT6P + $NADP^+$ $\longrightarrow$ RL5P+ NADPH + CO_{2c}
27. RL5P $\longrightarrow$ R5P
28. R5P $\longrightarrow$ XYL5P
29. R5P + XYL5P $\longrightarrow$ $\frac{7}{10}$ S7P + $\frac{3}{10}$ G3P
30. S7P + G3P $\longrightarrow$ $\frac{4}{10}$ E4P + $\frac{6}{10}$ F6P
31. XYL5P + E4P $\longrightarrow$ $\frac{6}{9}$ F6P + $\frac{3}{9}$ G3P

Lipid Synthesis

32. CIT_m $\longrightarrow$ CIT
33. CIT + ATP_c + CoA $\longrightarrow$ AcCoA + OXA + ADP
34. 8 AcCoA + 7 ATP_c + 14 NADPH $\longrightarrow$ Biomass + 14 $NADP^+$ + 7 ADP + 8 CoA

Mevalonate Pathway

35. 2AcCoA $\longrightarrow$ ACcCoA + CoA
36. ACcCoA +AcCoA $\longrightarrow$ HMG-CoA + CoA
37. HMG-CoA +2 NADPH $\longrightarrow$ MVA + 2 $NADP^+$
38. MVA + ATP_c $\longrightarrow$ MVA5P + ADP
39. MVA5P + ATP_c $\longrightarrow$ MVA5PP + ADP
40. MVA5PP + ATP_c $\longrightarrow$ IPP + ADP + CO_{2c}
41. IPP $\longrightarrow$ DMAPP
42. DMAPP $\longrightarrow$ IPP

Oxidative Phosphorylation

43. NADH + 3 O_2 $\longrightarrow$ 3ATP$_m$

44. FADH + 2 O_2 $\longrightarrow$ 2ATP$_m$

45. ADP + Pi $\longrightarrow$ ATP$_m$

46. ATP$_m$ $\longrightarrow$ ATP$_c$

Carotenoid Synthesis

47. 2 IPP $\longrightarrow$ GPP + PP

48. GPP + IPP $\longrightarrow$ FPP + PP

49. FPP + IPP $\longrightarrow$ GGPP + PP

50. 2 GGPP $\longrightarrow$ Phy + 2 PP

51. Phy + 3 $NADP^+$ $\longrightarrow$ NSR + 3 NADPH

52. NSR + $NADP^+$ $\longrightarrow$ LYC + NADPH

53. LYC $\longrightarrow$ γ-Car

54. γ-Car $\longrightarrow$ β-Car

55. β-Car + 2 NADPH + 2 O_2 $\longrightarrow$ ECNO + 2 $NADP^+$

56. ECNO + 3 NADPH + 3 O_2 $\longrightarrow$ PCX + 3 $NADP^+$

57. PCX + O_2 $\longrightarrow$ Ast

58. LYC + $NADP^+$ $\longrightarrow$ DHLYC + NADPH

59. DHLYC $\longrightarrow$ TOL

60. TOL + 2 O_2 + NADPH $\longrightarrow$ HDCO + $NADP^+$

61. β-Car + O_2 $\longrightarrow$ CRX

62. CRX + 2 NADPH + 3 O_2 $\longrightarrow$ ADX + 2 $NADP^+$

63. ADX + 2 NADPH + 2 O_2 $\longrightarrow$ Ast + 2 $NADP^+$

64. FPP + $NADP^+$ $\longrightarrow$ EGS + NADPH

Transhydrogenase Cycle

65. Pyr + ATP$_c$ + CO_{2c} $\longrightarrow$ OXA + ADP

66. OXA + NADH $\longrightarrow$ MAL + NAD^+

67. MAL + $NADP^+$ $\longrightarrow$ Pyr + NADPH + CO_{2c}

68. NAD^+ + ATP $\longrightarrow$ $NADP^+$ + ADP

69. MAL $\longrightarrow$ MAL_m

Protein Synthesis

70. Pyr $\longrightarrow$ 0.0825 Prot

71. E4P + PEP $\longrightarrow$ 0.0788 Prot

72. Pyr + AcCoA $\longrightarrow$ 0.2252 Prot

73. OXA $\longrightarrow$ 0.173 Prot

74. AKG $\longrightarrow$ 0.1609 Prot

75. 3PG $\longrightarrow$ 0.15 Prot

76. R5P $\longrightarrow$ 0.0228 Prot

77. GLUT $\longrightarrow$ 0.0675 Prot

78. GLA $\longrightarrow$ 0.0393 Prot

Gases Transfer Cell-Media

79. CO_{2c} $\longrightarrow$ CO_2

80. O_2 $\longrightarrow$ O_{2c}

Ammonium Assimilation

81. NH_3 $\longrightarrow$ NH_{3m}

82. NH_{3c} + AKG + NADPH $\longrightarrow$ GLUT + $NADP^+$

83. NH_{3c} + GLUT + ATP_c $\longrightarrow$ GLA + ADP

Structural Carbohydrates Synthesis

84. NH_{3c} + GLA + AcCoA + F6P + 2 ATP_c $\longrightarrow$ Carbs + 2 ADP

Synthesis of Nucleic Acids

85. 8 R5P + 4 OXA + 4 3PG + 64 ATP_c + 36 NH_{3c} + 11 NADPH $\longrightarrow$ Biomass + 12 NADH

References

[1] Mortimer P. Starr Arthur G. Andrewes Herman J. Phaff˙ CAROTENOIDS OF PHAFFlA RHODOZYMA, A RED-PIGMENTED FERMENTING YEAST. *Phytochemistry*, 15:1003/1007, August 1976.

[2] Estrada C. Kosalkova K. Barreiro C. Barredo, J. Biosynthesis of Astaxanthin as a Main Carotenoid in the Heterobasidiomycetous Yeast Xanthophyllomyces dendrorhous. *Journal of Fungi*, 3(44), July 2017.

[3] Koyunoglu C˙ Cancer cell growth - a mini review part-2: Crabtree effect, pasteur effect, pyruvate kinasetrient. *Biochemistry Analytical Biochemistry*, 7(4), December 2018.

[4] Cysewski Gerald Cappeli Bob Bagchi Debasis˙ Synthetic astaxanthin is significantly inferior to algal-based astaxanthin as an antioxidant and may not be suitable as a human nutraceutical supplement. *NutraFoods*, pages 126–133, December 2013.

[5] Flores-Cotera L Chavéz-Cabrera C Bustamante-Flores Z˙ Una Vista Integral de la Síntesis de Astaxantina en Phaffia rhodozyma. *BioTecnología*, 14(3), 2010.

[6] Marsch R Del Carmen Montes M Sánchez S Cacino-Díaz J Flores-Cotera L Chavéz-Cabrera C Bustamante-Flores Z˙ ATP-citrate lyase activity and carotenoid production in batch cultures of Phaffia rhodozyma under nitrogen-limited and nonlimited conditions. *Applied Microbiology and Biotechnology*, (85):1953–1960, September 2010.

[7] Jens Nielsen Urs von Stockar Christopher Cannizzaro Bjarke Christensen˙ Metabolic network analysis on phaffia rhodozyma yeast using 13 c–labeled glucose and gas chromatography-mass spectrometry. *Metabolic Engineering*, 6:340–351, July 2004.

[8] Paul D. Fraser Eugenio Alcalde˙ Extending our tools and resources in the non-conventional industrial yeast Xanthophyllomyces dendrorhous through the application of metabolite profiling methodologies. *Metabolomics*, 14(30), February 2018.

[9] Koroleff F. Determineation of ammonia. In Methods of Seawater Analysis. pages 126–133, December 1976.

[10] Ratledge F. Regulation of lipid accumulation in oleaginous microorganism. *Biochemical Society Transactions*, 30(6):1047–1050, June 2002.

[11] Eric A. Johnson Gil-Hwan An Myung-Haing Cho˙ Monocyclic Carotenoid Biosynthetic Pathway in the Yeast phaffia rhodozyma (Xanthophyllomyces dendrorhous) . *Journal of Bioscience and Bioengineering*, 88(2):189–293, April 1999.

[12] Jens Nielsen Gregory N. Stephanopoulos Aristos A. Aristidou˙ *Metabolic Engineering Principles and Methodologies*. Academic Press, 1998.

[13] Jan C. Verdoes Hans Visser Albert J.J. van Ooyen˙ Metabolic engineering of the astaxanthin-biosynthetic pathway of Xanthophyllomyces dendrorhous. *FEMS Yeast Research*, 4:221–231, July 2017.

[14] Telling R. C. Herbert D. Elsworth R.˙ The continuous culture of bacteria; a theoretical and experimental study. *Microbiology*, 14:601–622, 1956.

[15] Sören Gassel Chao Jin John Buckingham Markus Hümbelin Gerhard Sandmann Jens Schrader Isabell Schmidt Hendrik Schewe˙ Biotechnological production of astaxanthin with Phaffia rhodozyma/Xanthophyllomyces dendrorhous . *Applied Microbiology Biotechnology*, 89:555–571, September 2011.

[16] Nielsen J. Kayikcil O.˙ Glucose repression in Saccharomyces cerevisiae. *FEMS Yeast Research*, July 2015.

[17] Gross G. Lockwood S.˙ Disodium disuccinate astaxanthin (cardax^{TM}):antioxidant and antiinflammatory cardioprotection. *Cardiovascular Drug Reviews*, 23(3):199–216, 2005.

[18] Piret E. Luedeking R.˙ A kinetic study of the lactic acid fermentation. batch process at controlled ph. *Journal of Biochemicaland Microbiological Technology and Engineering*, 1(4):393–412, 1959.

[19] Nielsen J. Villadsen J. Nissen T. L. Schulze U.˙ Flux distributions in anaerobic, glucose-limited continuous cultures of saccharomyces cerevisiae. *Microbiology*, 143:203–218, 1997.

[20] Gerken H Lu Y Ling XPȧn X Wang B˙ Proteomic analysis of astaxanthin biosynthesis in Xanthophyllomyces dendrorhous in response to low carbon levels. *Bioprocess Biosystem Engineering*, (40):1091–1100, September 2017.

[21] Jennifer Alcaíno Marcelo Baeza1 Víctor Cifuentes Pilar Martinez-Moya1 Karsten Niehaus˙ Proteomic and metabolomic analysis of the carotenogenic yeast Xanthophyllomyces dendrorhous using different carbon sources. *BMC Genomics*, 16(289), 2015.

[22] Sabine Steiger Xiaojuan Xia Robert Bauer Gerhard Sandmann Marco Thines Rahul Sharma Sören Gassel˙ The genome of the basal agaricomycete Xanthophyllomyces dendrorhous provides insights into the organization of its acetyl-CoA derived pathways and the evolution of Agaricomycotina. *BMC Genomics*, 16(233), 2015.

[23] W̃eerasinghe D. Jolly S. Sedmak, J. Extraction and quantitation of astaxanthin from phaffia rhodozyma. *Biotechnology Techniques*, 4(2):107–112, 1990.

[24] Nielsen S.S. *Food Analysis Laboratory Manual*. Food Science Texts Series. Springer, 2010.

[25] Gerhard Sandmann Sören Gassel Jürgen Breitenbach˙ Genetic engineering of the complete carotenoid pathway towards enhanced astaxanthin formation in xanthophyllomyces dendrorhous starting from a high-yield mutant. *Applied Microbiology and Biotechnology*, 98:345–350, November 2013.

[26] Isabell Schmidt Jens Schrader Gerhard Sandmann Sören Gassel Hendrik Schewe˙ Multiple improvement of astaxanthin biosynthesis in Xanthophyllomyces dendrorhous by a combination of conventional mutagenesis and metabolic pathway engineering. *Biotechnology Letter*, 35:565–569, November 2012.

[27] Morita Toshihiko Nishimura Akima Sasaki Daisuke Ishhii Jun Ogino Chiaki Kizaki Noriyuki Kondo Akihiko Yamamoto Keisuke Hara Kiyotaka˙ Enhancement of astaxanthin production in Xanthophyllomyces dendrorhous by efficient method for the complete deletion of genes. *Microbial Cell Factories*, 15(155), 2016.

[28] Jian Yong Wu Yuan Shuai Liu˙ Modeling of Xanthophyllomyces dendrorhous Growth on Glucose and Overflow Metabolism in Batch and Fed-Batch Cultures for Astaxanthin Production. *Biotechnology and Bioengineering*, 101(5):996–1004, December 2008.

7 Vita

Victor Ignacio Martínez Castro was born on august 1^{st}, 1994 in Mexico, Mexico. During his early years showed interest in life sciences and engineering. On 2013 he obtained his diploma of Multicultural Baccalaureate in Instituto Tecnológico y de Estudios Superiores de Monterrey (ITESM) Campus Toluca. Later on he obtained a scholarship to study in the same Campus and obtained his Biotechnology engineering degree with minor in Bioprocesses on May 2018. Since the moment he entered the program he was accepted to form part of research projects and had the opportunity to present a poster in high density continuous culture of *Xanthophyllomyces dendrorhous* in a stirred tanked reactor in the iberoamerican congress of biotechnology "Bio Iberoamérica" on June 2016. He was accepted in the graduate program in Biotechnology in December 2018 in which he study the metabolic fluxes distribution in *X. dendrorhous* to understand the production of astaxanthin. During this period he was trained to work with different laboratory and pilot equipment, also he learned different methodologies to design experiments as well as a broader perspective in the metabolic engineering applications.

This document was typed using Overleaf a LaTeX compiler by Victor Ignacio Martínez Castro.